4

Applications of the fractional Fourier transform to optical pattern recognition

David Mendlovic, Zeev Zalevsky, and Haldun M. Ozaktas

4.1 Preface

Pattern recognition plays a major role in machine vision, robotics, automation, and image understanding. In particular, because of its high parallel processing capabilities, optics might be an excellent tool for achieving advantageous pattern recognition systems. During the recent four decades, intensive activities have been performed in order to demonstrate attractive optical pattern recognition systems. Nevertheless, final results, although they were quite impressive, did not succeed in massively introducing optics to the practical optical pattern recognition field.

One explanation for that phenomenon is the fact that optical pattern recognition is not flexible enough, especially compared with digital signal processing systems. Moreover, optical pattern recognition systems are commonly restricted to perform only correlation-type operations.

A recent approach to introducing more flexibility into optical pattern recognition systems is the use of the fractional-Fourier-transform operation that leads to so-called fractional correlation systems.

As a generalization of the conventional correlation, fractional correlation is a much more flexible tool that handles various types of missions with high efficiency. In this chapter, after the introduction of the fractional correlation and its optical implementations, a detailed performance analysis of it is given with respect to standard performance criteria. Then the space-variance–invariance property of the fractional correlation operation is discussed, and a real-time control of the space-invariance property is proposed. This resulted in a more flexible tool that is a fractional correlator with multiple fractional orders (the localized fractional processor). A particular example of the multiple fractional order processor is the anamorphic fractional processor that has also been demonstrated experimentally. The final stage toward higher flexibility is the fractional joint transform correlator that provides a real-time ability in a wider sense.

4.2 Introduction

One of the first practical optical approaches for performing correlation is the well-known VanderLugt 4-f coherent configuration [1], its analogous incoherent system [2] or the joint transform correlator (JTC) [3, 4]. Because conventional correlation is a shift-invariant operation, shifts of the input pattern provide a shifted correlation output plane with no effect on the field distribution, and pixels located close to the center have exactly the same effect as pixels located in the outer area.

In several pattern recognition applications, the shift-invariance property within the entire input plane is not necessary and can even be disturbing. An example is the case in which the object is to be recognized only when its location is inside a certain area and rejected otherwise, e.g., a label that has been affixed on the incorrect place during manufacturing. Several approaches for obtaining such space-variance detection have been suggested. The first approach is the tandem component processor that trades the shift invariance with high efficiency and a high peak-to-correlation-energy (PCE) ratio [5]. A different approach is based on a coded phase processor that multiplexes many filters and yet keeps the space–bandwidth product of the ordinary single-filter correlator [6]. Recently a space-variant Fresnel-transform correlator [7], which is closely related to a lensless intensity correlator [8], was suggested.

A similar approach is the fractional correlator (FC), whose optical implementation is made with a setup similar to that of the VanderLugt correlator [9, 10]. In contrast to the solution of using an appropriate input pupil that is open in the desired location, the FC does not require any additional equipment for its optical implementation. The FC itself selects the area of interest within the input scene. An additional example of the necessity of the FC is the case in which the recognition should be based mainly on the central pixels and less on the outer pixels (for example, in systems whose spatial resolution is improved in the central pixels and thus the central region of pixels is more reliable for the recognition process). An important application for the FC might be the detection of localized objects by use of a single cell detector, eliminating the need for a CCD array detector.

Fractional correlation is a generalization of the conventional correlation operation, and it is based on the fractional Fourier transform (FRT) [11]. The FRT operation is useful for various spatial filtering and signal processing applications [12, 13], that is, it is defined through a transformation kernel, as illustrated in Ref. 13:

$$[\mathcal{F}^p u(x)](x) = \int_{\infty}^{-\infty} B_p(x, x')u(x')\,dx', \tag{4.1}$$

where $B_p(x, x')$ is the kernel of the transformation and p is the fractional order:

$$B_p(x, x') = \frac{\exp\left\{-i\left[\frac{\pi \operatorname{sgn}(\sin\phi)}{4} - \frac{\phi}{2}\right]\right\}}{|\sin\phi|^{\frac{1}{2}}} \exp\left(i\pi \frac{x^2 + x'^2}{\tan\phi} - 2i\pi \frac{xx'}{\sin\phi}\right), \qquad \phi = \frac{p\pi}{2}. \tag{4.2}$$

This kernel has two optical interpretations: one is propagation through a gradient-index medium [11] and the second is a rotation operation applied over the Wigner plane [14]. Both definitions were shown to be fully equivalent in Ref. 15.

Based on the conventional correlation definition (performing a Fourier transform of both objects, taking the complex conjugate of one of the objects, multiplying the results, and finally performing an inverse Fourier transform), a definition of the FC was formulated: Performing a fractional Fourier transform of both objects, taking the complex conjugate of one of the objects, multiplying the results, and finally performing an inverse conventional Fourier transform. This definition for the FC is not the only definition, but it is one that was found to have many useful properties and successful applications [9]. The FC operation allows us to control the amount of the shift-variance property of the correlation. This property is based on the shift variance of the FRT, and it is more significant for the fractional orders of

$p \approx 0 + 2N$ and less for $p \approx 1 + 2N$ (N is any integer). Note that because the conventional Fourier transform is a special case of the FRT (a FRT with a fractional order of 1 becomes the conventional Fourier transform), the FC is automatically at least as good as the ordinary correlator because it includes the other as a special case and adds another additional degree of freedom. In Section 4.2 the performances of the FC are evaluated according to three main criteria: the signal-to-noise ratio (SNR) [16], the PCE ratio [17], and the Horner efficiency [18].

In the shift-variant correlation approaches, in order to obtain a correlator with a certain space variance, the length of the optical setup or the focal lengths of the lenses should be designed properly (in order to obtain the appropriate fractional orders that correspond to a certain amount of space variance). The filter placed in the fractional Fourier domain contains the FRT of a certain fractional order of the reference object. In order to change the amount of space variance, the fractional orders of the correlator should be changed too. This is done by changing the distances and the focal lengths of the lenses. Because the filter contains a different FRT order of the reference object, it must be recalculated. In Section 4.3, this necessity is overcome by the introduction of a different setup for performing a partial space-variant correlation [19]. In this approach, in order to change the amount of the space variance, one should change only the longitudinal location of the filter. The distances between the optical elements and the focal lengths of the lenses should not be changed. Also, the filter should not be recalculated or reencoded. It remains the same filter, and only its longitudinal location is changed.

Another area for which the FC has a promising potential is noise removal. One can assume an object that appears with several islands of chirp noise, each one with different parameters. Thus, a FRT with a varied order (as a function of the localization at the input plane), is required. This procedure is coined here as the localized FRT (LFRT) [20]. The LFRT may be also used in problems of pattern recognition in which a different amount of shift invariance is needed in different areas of the input plane. A common case in which different space-variant processing is required is related to fingerprint recognition [21]. The fingerprint is a pattern whose space variance is changed with the spatial location. The central region of the pattern is more or less constant, whereas the outer region of the fingerprint is changed from instant to instant because one never presses a finger with equal force. Thus, in order to recognize or reconstruct those prints, one requires a processor whose spatial shift variance is changeable. The amount of invariance needed for spatial shifting must be small in the center, but in the outer regions of the print, increasing shift invariance is required from the processor. In this practical case, a LFRT processor should be helpful. The LFRT processor as well as its possible applications are discussed in Section 4.4.

Recently the FRT operation has been also extended to the anamorphic case [22, 23]. This provides the possibility of independently varying the space variance of the system in two perpendicular directions. In Section 4.5, a flexible system for obtaining an anamorphic-based fractional correlation is proposed. It is based on an adjustable-scale anamorphic FRT transformer, followed in cascade by a second transformer that, depending on the codification of the filter, can be amorphic or anamorphic [24]. The system is employed for space-variant processing, which implements multiple targets to be detected in different zones of the image.

As mentioned above, another approach for performing an optical spatial image process is the JTC. This scheme does not contain any filter and thus provides some advantages compared with the conventional VanderLugt 4-f configuration, in which the filter should be generated in a complex process, and must be aligned with high accuracy. When the shift invariance of the input plane is not important, a fractional JTC

configuration may be used [25]. This configuration is analyzed in Section 4.6. The advantages of such a configuration in the optical pattern recognition field are similar to the advantages of the conventional JTC approach, but in addition the amount of the shift invariance may be controlled.

4.3 Fractional correlator performance analysis

In order to indicate the advantages of the FC configuration, its performance has been examined. This examination was done according to common performance criteria, which are described below.

4.3.1 Performance criteria

In this subsection three main performance criteria are presented: the SNR [16], the PCE ratio [17], and the Horner efficiency [18]. The advantage of using the above criteria over other common criteria such as the peak-to-maximum-sidelobe ratio [26] is that they may be easily analyzed mathematically.

The SNR measures the sensitivity of the autocorrelation peak to additive noise at the input plane. Mathematically,

$$\mathrm{SNR} = \frac{|E[C_{u,u+n}(0)]|^2}{\mathrm{VAR}[C_{u,u+n}(0)]}, \tag{4.3}$$

where u is the input signal, n is an additive noise, and $C_{u,v}$ is the correlation between u and v where in Eq. (4.3) $v = u + n$. E denotes the expected value operator, and VAR is the variance over the ensemble $n(x)$ [27].

The SNR measure considers only the average and the variance of the correlation peak but not the shape of the correlation output. The shape is estimated by the PCE criterion that measures the sharpness of the correlation peak. Its mathematical definition is

$$\mathrm{PCE} = \frac{|C_{u,v}(0)|^2}{E_c}, \tag{4.4}$$

where E_c is the energy of the correlation signal defined by

$$E_c = \int_{-\infty}^{\infty} |C_{u,v}(x)|^2 \, \mathrm{d}x. \tag{4.5}$$

From Eqs. (4.5) and (4.4), it is seen that for sharp correlation peaks, the value of the PCE is large.

The criterion that measures the light efficiency is the Horner efficiency criteria. It describes the ratio between the total light energy in the output plane and the total light energy in the input plane:

$$\eta = \frac{\int_{-\infty}^{\infty} |C_{u,v}(x)|^2 \, \mathrm{d}x}{\int_{-\infty}^{\infty} |u(x)|^2 \, \mathrm{d}x}. \tag{4.6}$$

However, Horner later recommended another definition for η [28]:

$$\eta = \frac{|C_{u,v}(0)|^2}{\int_{-\infty}^{\infty} |u(x)|^2 \, \mathrm{d}x}. \tag{4.7}$$

This definition is much more relevant for correlators because the significant output of a correlator is the energy of the correlation peak itself $[|C_{u,v}(0)|^2]$ and not the energy of the entire correlation plane.

4.3.2 Performance optimization in conventional correlators

Various filtering configurations exist in the literature [1, 17, 29], and each optimizes another performance criterion.

The matched filter (MF) H_{MF} optimizes the SNR measure:

$$H_{\mathrm{MF}}(\nu) = \alpha \frac{U^*(\nu)}{P_n(\nu)}, \tag{4.8}$$

where α is a constant that does not affect the SNR, P_n denotes the power spectral density of the noise $n(x)$, and U is the Fourier transform of the reference object. For the special case of white noise, $P_n = N_0$ (a constant), one obtains

$$H_{\mathrm{MF}}(\nu) = \beta U^*(\nu), \tag{4.9}$$

where $\beta = (\alpha/N_0)$ (constant).

The filter type that is optimal according to the PCE measure is the inverse filter (IF), which is defined by

$$H_{\mathrm{IF}}(\nu) = \frac{U^*(\nu)}{|U(\nu)|^2}. \tag{4.10}$$

Intuitively, when the IF is used and the input is the reference object, the correlation signal is a delta function (by design); thus the PCE ratio is the highest. However, the main disadvantage of the IF is that it may contain infinite values.

The phase-only filter (POF) is defined by

$$H_{\mathrm{POF}}(\nu) = \frac{U^*(\nu)}{|U(\nu)|} \tag{4.11}$$

and is known to optimize the Horner efficiency measure [17]. The intuitive explanation is that the POF does not attenuate the energy passing through the filter, as $|H| = 1$.

4.3.3 Performance optimization in fractional correlators

In order to investigate which filtering configuration is optimal in the FC case, the fractional power filter (FPF) term [17] has to be introduced. Note that in this term there is no connection with the FRT although the name FPF could be confusing. The FPF definition is a generalization of the various filters (MF, IF, and POF) presented above:

$$H_{\mathrm{FPF}}(\nu) = |U(\nu)|^s \exp[-i\theta(\nu)] = |U|^{s-1}U^*, \tag{4.12}$$

where $U(\nu) = |U(\nu)| \exp[i\theta(\nu)]$. The value of the s parameter can be any real number. The MF, POF, and IF are obtained with $s = +1, 0$, and -1, respectively.

For the FC case we used the schematic sketch of Fig. 1 for the configuration of the FC. We chose the parameters of $p_1 = p$, $p_2 = -p$, and $p_3 = -1$.

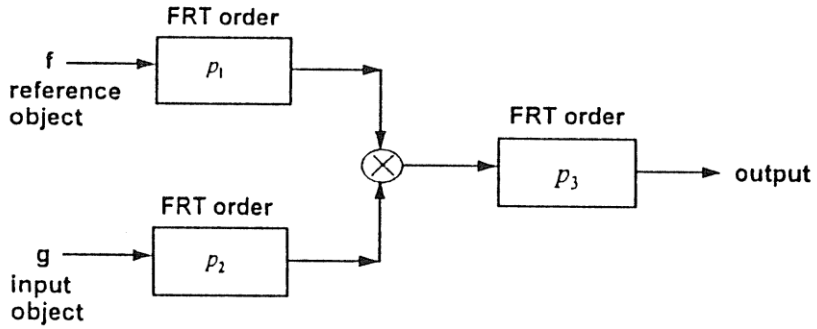

Fig. 4.1. Schematic sketch of the FRT filtering system.

Note that, for real input objects, choosing $p_2 = -p$ is equivalent to performing a FRT with the fractional order of p and applying the complex conjugate over the transformed function.

The FRT of the reference function $u(x)$ is denoted by $\mathcal{F}^p u(x) = u_p(x_p)$. The resultant FPF filter is given by

$$H(x_p) = |u_p(x_p)|^{s-1} u_p^*(x_p). \tag{4.13}$$

The SNR measure can be obtained with Eq. (4.3) as

$$\mathrm{SNR} = \frac{\left| \int_{-\infty}^{\infty} H(x_p) u_p(x_p)\, \mathrm{d}x_p \right|^2}{\int_{-\infty}^{\infty} P_n(x_p) |H(x_p)|^2\, \mathrm{d}x_p}. \tag{4.14}$$

While dealing with input white noise $n(x)$, we find that the obtained noise energy density $P_n(x_p)$ is also white (see Subsection 4.3.6). Thus assuming $P_n(x_p) = N_0$ and using Eq. (4.13) result in

$$\mathrm{SNR} = \frac{\left[\int_{-\infty}^{\infty} |u_p(x_p)|^{s+1}\, \mathrm{d}x_p \right]^2}{N_p \int_{-\infty}^{\infty} |u_p(x_p)|^{2s}\, \mathrm{d}x_p}. \tag{4.15}$$

In order to maximize the SNR expression with respect to s, (dSNR)/ds is set to zero:

$$\begin{aligned} &\int_{-\infty}^{\infty} |u_p(x_p)|^{2s}\, \mathrm{d}x_p \frac{\mathrm{d}}{\mathrm{d}s} \left[\int_{-\infty}^{\infty} |u_p(x_p)|^{s+1}\, \mathrm{d}x_p \right]^2 \\ &\quad = \left[\int_{-\infty}^{\infty} |u_p(x_p)|^{s+1}\, \mathrm{d}x_p \right]^2 \frac{\mathrm{d}}{\mathrm{d}s} \int_{-\infty}^{\infty} |u_p(x_p)|^{2s}\, \mathrm{d}x_p. \end{aligned} \tag{4.16}$$

After differentiation with respect to s, the following result is obtained:

$$\frac{\int_{-\infty}^{\infty} |u_p|^{2s}\, \mathrm{d}x_p}{\int_{-\infty}^{\infty} |u_p|^{s+1}\, \mathrm{d}x_p} = \frac{\int_{-\infty}^{\infty} |u_p|^{2s} \ln(|u_p|)\, \mathrm{d}x_p}{\int_{-\infty}^{\infty} |u_p|^{s+1} \ln(|u_p|)\, \mathrm{d}x_p}. \tag{4.17}$$

The condition that maximizes the SNR [Eq. (4.17)] is satisfied for $s = 1$, which is the MF $H = u_p^*$.

The light efficiency of the FPF can be obtained from Eqs. (4.6) and (4.13) as

$$\eta = \delta \frac{\int_{-\infty}^{\infty} |u_p(x_p)|^{2(1+s)}\, \mathrm{d}x_p}{\int_{-\infty}^{\infty} |u_p(x_p)|^2\, \mathrm{d}x_p}, \tag{4.18}$$

where δ is a constant that is chosen so that the maximal magnitude of the FPF will be 1 (the filter is a passive device). After Eq. (4.18) is rewritten,

$$\eta = \delta \frac{\int_{-\infty}^{\infty} |H(x_p)u_p(x_p)|^2 \, dx_p}{\int_{-\infty}^{\infty} |u_p(x_p)|^2 \, dx_p} = \delta \frac{\int_{-\infty}^{\infty} |H(x_p)|^2 |u_p(x_p)|^2 \, dx_p}{\int_{-\infty}^{\infty} |u_p(x_p)|^2 \, dx_p}, \tag{4.19}$$

where H is the filter distribution. It is easy to see that if H is a passive filter, any filter with $|H| = 1$ (not just a POF) maximizes the light efficiency of Eq. (4.6). However, when the second definition of η [Eq. (4.7)] is used,

$$\eta = \delta \frac{\left| \int_{-\infty}^{\infty} |u_p(x_p)|^{(s+1)} \, dx_p \right|^2}{\int_{-\infty}^{\infty} |u_p(x_p)|^2 \, dx_p}, \tag{4.20}$$

rewriting Eq. (4.20) leads to

$$\begin{aligned} \eta &= \delta \frac{\left| \int_{-\infty}^{\infty} H(x_p)u_p(x_p) \, dx_p \right|^2}{\int_{-\infty}^{\infty} |u_p(x_p)|^2 \, dx_p} \\ &= \delta \frac{\left| \int_{-\infty}^{\infty} |H(x_p)| \exp[i\phi_H(x_p)] |u_p(x_p)| \exp[i\phi_u(x_p)] \, dx_p \right|^2}{\int_{-\infty}^{\infty} |u_p(x_p)|^2 \, dx_p}, \end{aligned} \tag{4.21}$$

where ϕ_H is the phase of H and ϕ_u is the phase of u_p. Under the condition of the passivity of H, the numerator is maximized if and only if $\phi_H = -\phi_u$ and $|H| = 1$, i.e., H is a POF.

The PCE of the FPF is obtained when Eqs. (4.4) and (4.13) are combined:

$$\text{PCE} = \frac{\left[\int_{-\infty}^{\infty} |u_p(x_p)|^{s+1} \, dx_p \right]^2}{\int_{-\infty}^{\infty} |u_p(x_p)|^{2(s+1)} \, dx_p}. \tag{4.22}$$

After setting the derivative of Eq. (4.22) with respect to s to zero, one obtains

$$\frac{\int_{-\infty}^{\infty} |u_p|^{2(s+1)} \, dx_p}{\int_{-\infty}^{\infty} |u_p|^{s+1} \, dx_p} = \frac{\int_{-\infty}^{\infty} |u_p|^{2(s+1)} \ln(|u_p|) \, dx_p}{\int_{-\infty}^{\infty} |u_p|^{s+1} \ln(|u_p|) \, dx_p}. \tag{4.23}$$

The above condition is satisfied for $s = -1$ (the IF) for any $|u_p(x_p)| > 0$. This result agrees with the conventional correlator, for which the IF is designed to generate a delta function at the correlation plane.

However, one should note that in the fractional case the PCE measure is not significant. The PCE is a measure for the peak sharpness; however, the FC is shift variant and thus the shape of the peak is irrelevant. In most cases the FC configuration may work with a single detector. The FC cannot be used for localization of the input object; it can tell only if the input object exists in some specific region. The only exception is for p values that are close to 1. Then the shift variance is very small and the peak sharpness is relevant.

4.3.4 Signal-to-noise ratio comparison between a fractional correlator and a conventional correlator

Here a comparison of the SNR performances for the FC and the conventional correlator is performed. In the derivations below, white input noise is assumed. According to the

Cauchy–Schwartz inequality, one may conclude that the correlation's peak magnitude for a matched filter $H = u_p^*$ is

$$C_{u,v}^{p}(0) = C_{u,v}^{1}(0), \tag{4.24}$$

where u and v are any arbitrary functions. Note that the SNR is a function of the correlation peak only and not of the whole correlation signal. When Eqs. (4.3) and (4.24) are combined it is easy to show that the SNR remains unchanged when the fractional order of the FC is varied:

$$\mathrm{SNR}_p = \mathrm{SNR}_1. \tag{4.25}$$

Equation (4.25) states an important feature: The SNR performance of the FC is exactly the same as that of the conventional correlator. Thus the shift-variance property of the correlator is achieved without decreasing the SNR performances.

4.3.5 Fractional correlator performance with additive colored noise

Any colored noise $n_c(x)$ can be constructed from white noise $n_0(x)$ with a power spectrum of $Sn_0(\nu) = N_0$ convolving it with a linear time-invariant filter $h(x)$. The obtained power spectrum is [27]

$$Sn_c(\nu) = E[|N(\nu)H(\nu)|^2] = E[|N(\nu)|^2]|H(\nu)|^2 = N_0|H(\nu)|^2, \tag{4.26}$$

where $N(\nu) = \mathcal{F}^1 n_0(x)$ and $H(\nu) = \mathcal{F}^1 h(x)$. $E[\cdot]$ denotes averaging over the ensemble of the noise samples [27]. The relation between the statistical autocorrelation function and the power spectrum of the colored noise is an inverse Fourier transform:

$$Rn_c(x_1, x_2) = Rn_c(\tau = x_1 - x_2) = \mathcal{F}^{-1} Sn_c(\nu). \tag{4.27}$$

To find the noise spectrum at the filter plane, let $n_p(x_p)$ denote the FRT of one sample of $n_c(x)$. According to Eq. (4.2) the relation between n_p and n_c is

$$n_p(x) = \int_{-\infty}^{\infty} n_c(x_0) \exp\left(i\pi \frac{x^2 + x_0^2}{T} - 2\pi i \frac{x x_0}{S} \right) \mathrm{d}x_0, \tag{4.28}$$

where

$$S = \sin\phi \qquad T = \tan\phi. \tag{4.29}$$

To find the power spectrum $Sn_p(\nu)$, one needs to write the autocorrelation function Rn_p:

$$Rn_p(x_1, x_2) = E\left[n_p(x_1) n_p^*(x_2) \right]. \tag{4.30}$$

By using Eqs. (4.28) and (4.29), one obtains

$$Rn_p(x_1, x_2) = \int_{-\infty}^{\infty} \int_{-\infty}^{\infty} E\left[n_c(x_1) n_c^*(x_2) \right] \exp\left(i\pi \frac{x_1^2 + x_0^2 - x_2^2 - x_0'^2}{T} - 2\pi i \frac{x_1 x_0 - x_2 x_0'}{S} \right) \mathrm{d}x_0 \, \mathrm{d}x_0'. \tag{4.31}$$

Note that $E[n_c(x_1)n_c^*(x_2)] = Rn_c(x_1 - x_2)$, and thus

$$Rn_p(x_1, x_2) = \int_{-\infty}^{\infty}\int_{-\infty}^{\infty} Rn_c(x_1 - x_2) \times \exp\left(i\pi\frac{x_1^2 + x_0^2 - x_2^2 - x_0'^2}{T} - 2\pi i\frac{x_1x_0 - x_2x_0'}{S}\right) dx_0\, dx_0'. \quad (4.32)$$

From Eq. (4.32) it is clear that Rn_p cannot be written as $Rn_p(x_1 - x_2)$, and thus Rn_p is a nonstationary random process. Because the usual Fourier-transform relation between the autocorrelation and the power spectrum does not hold for a nonstationary process, the following relation should be used instead [27]:

$$Sn_p(\nu) = \int_{-\infty}^{\infty} \langle Rn_p(x_1, x_1 + \Delta x)\rangle \exp(-i2\pi\nu\Delta x)\, d\Delta x, \quad (4.33)$$

where $\langle\cdot\rangle$ denotes averaging over x_1. This relation was used for calculating the noise power distribution for various fractional orders by means of a computer simulation. The input colored-noise shape is a low-pass noise with a Gaussian spectral shape. Figure 4.2 illustrates the power distribution after the FRT (at the filter plane) for various fractional orders.

The result was obtained by the averaging of 100 random colored-noise vectors (because the vector is finite for $p = 1$, no fine Gaussian was obtained). The purpose of Fig. 4.2 is to illustrate that the increment of the fractional order p narrows the spectral width of the noise.

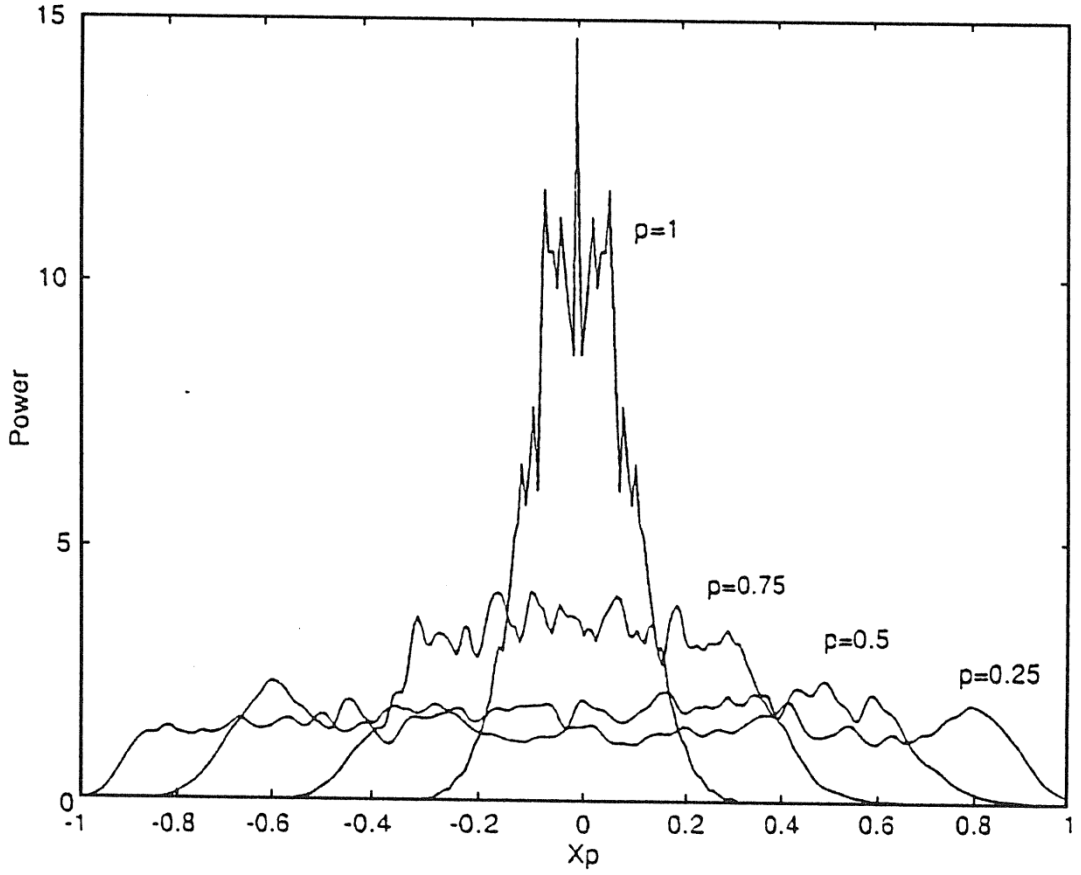

Fig. 4.2. Average power distribution for low-pass input noise.

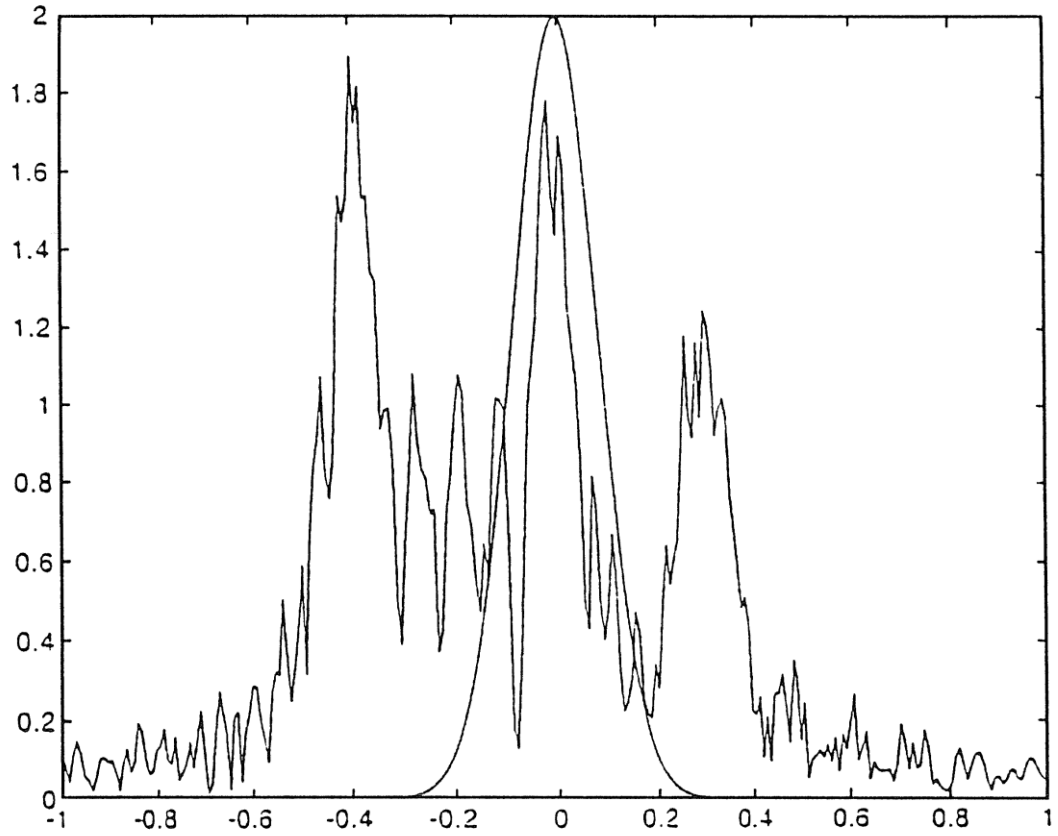

Fig. 4.3. Colored-noise and object power distribution at the filter plane for $p = 0.5$.

In Fig. 4.3, colored noise is assumed with a Gaussian shape at the fractional plane of $p = 0.5$. This Gaussian distribution is plotted in the middle of the figure. As the reference object, a bar-code pattern was assumed. The FRT magnitude of the reference object for $p = 0.5$ is also plotted in Fig. 4.3. According to the Perseval theorem, the integral over the overlapping area between the spectrum of the noise and the reference object equals the noise added to the correlation peak.

Consider a different reference object, for example, the same bar-code pattern but shifted along the x axis. The FRT magnitude is changed and shifted as shown in Fig. 4.4. Note that the overlapping area between the noise spectrum and the signal spectrum is reduced.

This example shows that the noise performance for the FC and the non-white-noise case is *object dependent*, which means that the correlation peak's sensitivity to the input noise is affected strongly by both the reference object and by its position. Note that, in the above simulations, the Gaussian shape distribution was chosen for the fractional plane of $p = 0.5$.

4.3.6 Fractional Fourier transform of white noise

The statistical autocorrelation of a zero-mean, stationary white-noise random process $n_0(x)$ is [27]

$$Rn_0(x_1, x_2) = N_0\delta(x_1 - x_2). \tag{4.34}$$

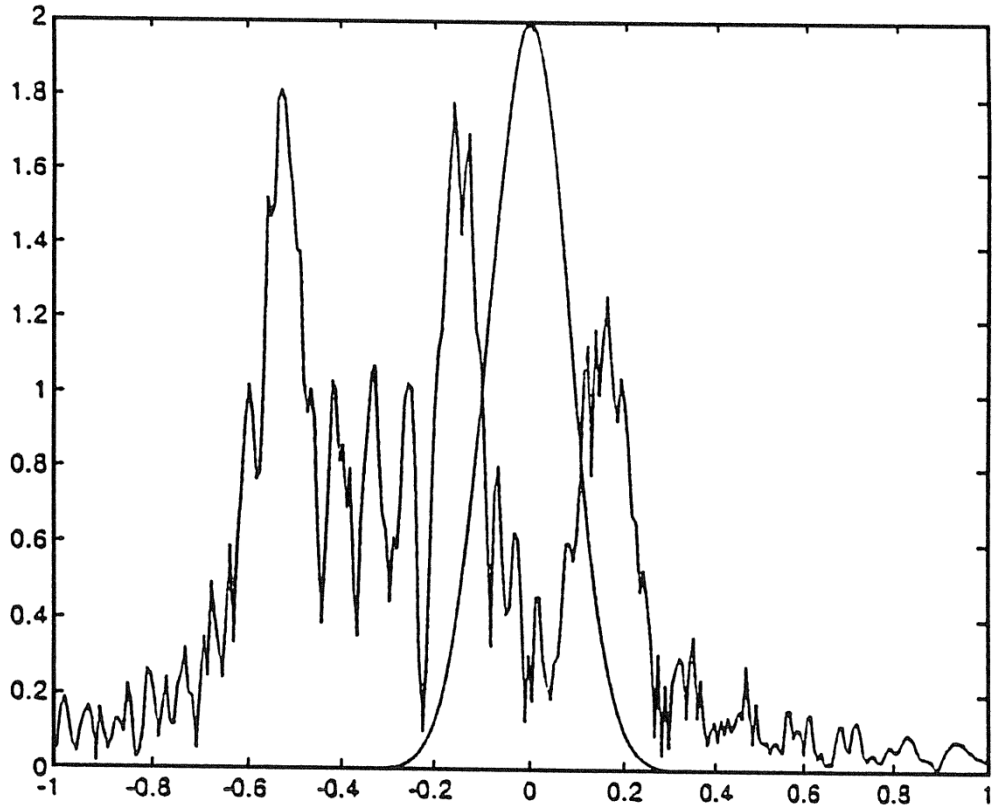

Fig. 4.4. Colored-noise and shifted object power distribution at the filter plane for $p = 0.5$.

The FRT of the white-noise input is denoted by $n_p(x)$. The statistical autocorrelation of $n_p(x)$ is

$$Rn_p(x_1, x_2) = E\left[n_p(x_1)n_p^*(x_2)\right]. \tag{4.35}$$

By using the FRT definition [Eqs. (4.2) and (4.29)], and changing the order of integration and expectation, one obtains

$$E[n_p(x_1)n_p^*(x_2)] = \int_{-\infty}^{\infty}\int_{-\infty}^{\infty} Rn_0(x, x') \exp\left(i\pi \frac{x^2+x_1^2-x'^2-x_2^2}{T} - 2i\pi \frac{xx_1-x'x_2}{S}\right) dx\, dx'. \tag{4.36}$$

When Eq. (4.34) is used, Eq. (4.36) becomes

$$E\left[n_p(x_1)n_p^*(x_2)\right] = N_0 \int_{-\infty}^{\infty} \exp\left(i\pi \frac{x_1^2 - x_2^2}{T} - 2i\pi x \frac{x_1 - x_2}{S}\right) dx, \tag{4.37}$$

which yields

$$Rn_p(x_1, x_2) = N_0\delta(x_1 - x_2). \tag{4.38}$$

With a similar derivation it is easy to show that for a zero-mean input noise, the output is zero mean as well:

$$E[n_p(x)] = 0. \tag{4.39}$$

Thus from Eqs. (4.38) and (4.39) it is clear that $n_p(x)$ is zero mean, stationary, and white.

4.4 Fractional correlator with real-time control of the space-invariance property

As mentioned above, the commonly known configurations for obtaining the FC are preliminary designed to obtain a FC with a predefined fractional order and a predefined filtering function. The distances between the optical elements and the focal lengths of the lenses are determined accordingly. In order to change the fractional order of the FC, one must change the distances between the elements of the setup and change the focal lengths of the lenses, and recompute the filter function. In this section we illustrate a new type of FC with real-time control of the space-invariance property. Here the amount of the shift variance (fractional order) is controlled only by the longitudinal position of the filter. In order to change the fractional order, one should vary the longitudinal position of the filter. The focal lengths of the lenses, the distances between them, and the filter's function should not be changed.

4.4.1 Mathematical analysis

The suggested FC with a real-time control of the space-invariance property is illustrated in Fig. 4.5. In this setup the parameter a (the longitudinal position of the filter) varies from 0 to 1, and it corresponds to the amount of the shift invariance (the fractional order of the correlator). In order to change the fractional order, one should vary the parameter a. The filter itself remains unchanged when the fractional order is varied. To prove this, let us first analyze the first part of the optical system of Fig. 4.5. In this part the input pattern $g(x)$ is first multiplied by a lens, transparency $\exp[(-i\pi x^2)/(\lambda f)]$, then it is propagated (with the Fresnel diffraction formula) by a distance af in the free space (f is the focal length of the lens). Now the field distribution is multiplied by the filter $F(u)$. $F(u)$ is the conventional Fourier transform of the reference impulse response. The result is again propagated a distance of $(1-a)f$ in the free space with the Fresnel diffraction formula. Another multiplication with a lens, $\exp[(-i\pi v^2)/(\lambda f)]$, is done. The second part of the system is simply a Fourier transform over the output of the first part.

After the above-mentioned mathematical analysis, the field distribution at the output of the first part of the system (at the Fourier plane) is

$$D(v) = C\exp\left[\frac{i\pi a v^2}{\lambda(1-a)f}\right]\int_{-\infty}^{\infty} F(u)Z(u) \times \exp\left[\frac{i\pi u^2}{\lambda a(1-a)f}\right]\exp\left[-2\pi i\frac{uv}{\lambda(1-a)f}\right]du, \tag{4.40}$$

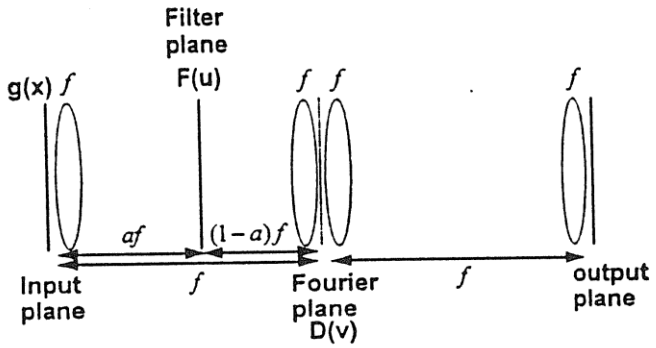

Fig. 4.5. Suggested optical filtering system.

where C is a constant and

$$Z(u) = \int_{-\infty}^{\infty} g(x) \exp\left[\frac{i\pi x^2\left(\frac{1}{a} - 1\right)}{\lambda f}\right] \exp\left[-2\pi i \frac{ux}{\lambda a f}\right] dx. \tag{4.41}$$

Note that in Eq. (4.2) a normalized coordinate set x_r (that has no physical dimensions) was used:

$$x_r = \frac{x_{ph}}{\sqrt{\lambda f}}, \tag{4.42}$$

where x_r is the normalized coordinate and x_{ph} is the physical coordinate. Note that the normalized set is good for mathematical analysis. However, because here we are dealing with physical implementation, the physical set must be used. A comparison between Eqs. (4.2) (in physical coordinates) and (4.41) shows that $\exp\{[i\pi(1-a)u^2]/[\lambda a(1-2a-2a^2)f]\}Z(u)$ is a scaled FRT of $g(x)$:

$$\exp\left[\frac{i\pi(1-a)u^2}{\lambda a(1-2a-2a^2)f}\right] Z(u) = \mathcal{F}^{p_1} g(x) = G_{p_1}(su); \tag{4.43}$$

the fractional order is notated by p_1, and s is the scaling factor. The relation between the a parameter and the fractional order p_1 can be easily derived again from the comparison between Eqs. (4.2) and (4.41):

$$\tan\frac{p_1\pi}{2} = \frac{1}{\frac{1}{a} - 1} = \frac{a}{1-a}, \tag{4.44}$$

and the scaling factor s is found to be

$$s = \frac{\sin\frac{p_1\pi}{2}}{a} = \frac{1}{\sqrt{1-2a+2a^2}}. \tag{4.45}$$

Note that the quadratic exponent $\exp\{[i\pi(1-a)u^2]/[\lambda a(1-2a-2a^2)f]\}$ that multiplies $Z(u)$ in Eq. (4.43) was determined to fit the quadratic exponent $\exp\{(i\pi x^2)/[\lambda f \tan(p_1(\pi/2))]\}$ appearing in Eq. (4.2) (after the scaling factor $x = su$ was substituted).

Thus Eq. (4.41) may be rewritten as

$$D(v) = C' \exp\left[\frac{i\pi a v^2}{\lambda(1-a)f}\right] \int_{-\infty}^{\infty} F(u) G_{p_1}(su) \exp\left(\frac{i\pi L u^2}{\lambda f}\right) \exp\left[-2\pi i \frac{uv}{\lambda(1-a)f}\right] du, \tag{4.46}$$

where C' is a constant and

$$L = \frac{1}{a(1-a)} - \frac{1-a}{(1-2a+2a^2)a} = \frac{a}{(1-a)(1-2a+2a^2)}. \tag{4.47}$$

Rewriting Eq. (4.47) leads to

$$D(v) = C'' \exp\left[\frac{i\pi a v^2}{\lambda(1-a)f}\right] \int_{-\infty}^{\infty} F(u) G_{p_1}(su) \times \exp\left[\frac{i\pi(su)^2 \frac{L}{s^2}}{\lambda f}\right] \exp\left[-2\pi i \frac{su\frac{v}{s}}{\lambda(1-a)f}\right] d(su), \tag{4.48}$$

where C'' is a constant. After changing the integration variables to $u' = su$, one obtains

$$D(v) = C'' \exp\left[\frac{i\pi a v^2}{\lambda(1-a)f}\right] \int_{-\infty}^{\infty} F\left(\frac{u'}{s}\right) G_{p_1}(u') \times \exp\left[\frac{i\pi u'^2 \frac{L}{s^2}}{\lambda f}\right] \exp\left[-2\pi i \frac{u'v}{\lambda v(1-a)f}\right] du'. \tag{4.49}$$

Another comparison between Eqs. (4.2) (in physical coordinates) and (4.48) shows that Eq. (4.48) is an exact FRT of the order of p_2 over the multiplication between the scaled filter $F(u/s)$ and $G_{p_1}(u)$ [the FRT of the order of p_1 over $g(x)$]:

$$\tan\frac{p_2\pi}{2} = \frac{s^2}{L} = \frac{1-a}{a}; \tag{4.50}$$

thus

$$\tan\frac{p_2\pi}{2} = \frac{1}{\tan\frac{p_1\pi}{2}}, \tag{4.51}$$

which means that

$$p_2 = 1 - p_1. \tag{4.52}$$

Thus a FRT of the order of p_2 is applied over the multiplication between $F(u/s)$ and $G_{p_1}(u)$ [the FRT of the order of p_1 of $g(x)$]. Because $F(u/s) = \mathcal{F}^1 f(sx)$, the setup performs a fractional correlation between the scaled reference object $f(sx)$ and the input object $g(x)$. Because the second part of the optical setup performs a conventional Fourier transform, the flow chart of the system can be illustrated, as was done in Fig. 4.1, choosing $p_1 = 1$, $p_2 = p$, and $p_3 = 2 - p$.

4.4.2 Interpretations

The most general schematic sketch for the fractional correlator is shown in Fig. 4.1. For this configuration a condition was derived for the fractional correlator that is optimal according to the PCE criteria [30]:

$$\frac{1}{T_1} + \frac{1}{T_2} + \frac{1}{T_3} = 0, \tag{4.53}$$

where

$$T_k = \tan\phi_k, \qquad \phi_k = p_k(\pi/2), \qquad k = 1, 2, 3. \tag{4.54a}$$

According to Subsection 4.4.1, which illustrated the equivalence between the suggested optical setup and the flow chart of Fig. 4.1 (for $p_1 = 1$, $p_2 = p$, and $p_3 = 2 - p$), one can easily see that the condition of Eq. (4.53) is fulfilled. To examine the applicability of a FC with parameters $p_1 = p$, $p_2 = 1$, and $p_3 = 2 - p$, let us first investigate the mathematical expression of the correlation plane. If the input object is indicated by $g(x)$ and the reference object by $f(x)$, the mathematical expression for the output of general FC (see Fig. 4.1) is, according to [30]:

$$|V(x)| = \left| \int g(x_1) f\left(\frac{-x_1}{\sin\phi} - \frac{x}{\sin\phi}\right) \exp\left[i\pi\left(\frac{x_1^2}{\tan\phi}\right)\right] dx_1 \right|. \tag{4.54b}$$

Assuming that the input is shifted and illuminated by a converging spherical wave, one obtains

$$g(x) = u(x - x_0)\exp\left[-i\pi\frac{(x - x_0)^2}{\tan\phi}\right], \tag{4.54c}$$

where u is the object we wish to recognize and x_0 is the relative lateral shift between the reference object encoded in the filter and the input pattern. Assuming also that the filter is $f(x) = u^*(-x\sin\phi)$ one easily finds that

$$|V(x)| = \left|\int u(x_1 - x_0)u^*(x_1 + x)\exp\left(\frac{2\pi i x_1 x_0}{\tan\phi}\right)\mathrm{d}x_1\right|. \tag{4.54d}$$

Observing the last expression reveals that the ideal peak is obtained if $x_0 = 0$. The location of this peak is on $x = 0$ and it will not depend on the fractional order. However, if x_0 is not zero a disturbing phase factor appears in the exponential term that will attenuate the peak if the shift x_0 is too big.

Another ability of this configuration is as a noise-removing filter for an additive chirp-type noise. This time the input should be illuminated by a plane wave (and not a converging spherical wave) and $F(u)$ should be a notch filter (all pass filter that blocks only the axis center coordinate in order to remove the delta obtained in the filter plane due to the transformed chirp-type noise).

4.5 Localized fractional processor

The FC discussed so far was based on the FRT with a uniform fractional order applied over the reference and the input functions. In this section we introduce a localized FRT (LFRT), i.e., a FRT whose fractional order is space dependent, and thus the amount of shift variance–invariance is also spatially controlled. Such a transformation may be implemented optically in FC configurations, that achieving both shift-variant noise removal (for nonstationary noises whose statistical properties are varied with the spatial position) and image detection (for many detection applications that could be implemented with better efficiency by shift-variant or partially shift-variant processors).

4.5.1 Mathematical definitions

The basic assumption of the LFRT is that there is a full spatial separation between the areas that require different FRT orders. Thus we suggest, as a preliminary action, splitting up the different areas into different spatial locations. Assuming an input signal $f(x, y)$ and writing it as a separation of independent areas (as shown in Fig. 4.6) gives

$$f(x, y) = \sum_{i=1}^{i=N} f(x, y)A_i(x, y). \tag{4.55}$$

Each spatial area that is supposed to be transformed with a different fractional order is called a channel. The separation between the channels is achieved by the encoding of every area $A_i(x, y)$ with a different spatial frequency. Thus, after applying the FRT operation, one obtains

$$\mathrm{OUT}(u, v) = \sum_{i=1}^{i=N}\left[G_i(u, v)\int_{-\infty}^{\infty} f(x, y)A_i(x, y)B_{p_i}(u, v; x, y)\,\mathrm{d}x\,\mathrm{d}y\right], \tag{4.56}$$

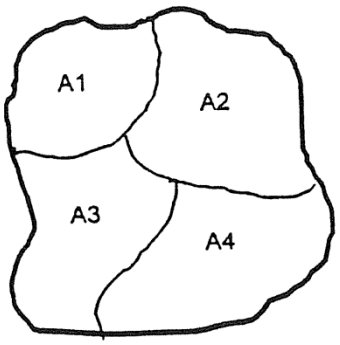

Fig. 4.6. Writing the signal as a separation of independent areas.

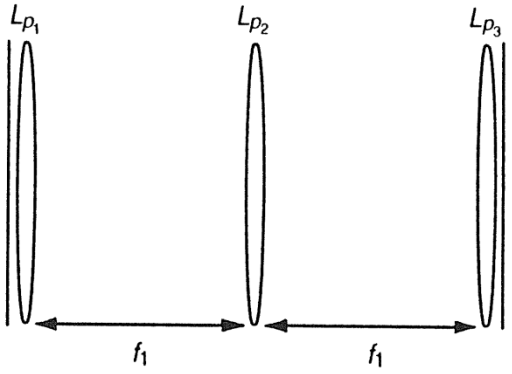

Fig. 4.7. Optical setup for obtaining a FRT with fixed distances and varying orders.

where $B_{p_i}(u, v; x, y)$ is the two-dimensional FRT kernel, p_i is the space-variant fractional order, and $G_i(u, v)$ is the independent output area in which the LFRT is obtained.

In the proposed processor we use the FRT optical configuration that is presented in Fig. 4.7. Here, the distances are fixed for all fractional orders and only the focal lengths of the lenses are varied for changing the FRT order.

The validity of this setup was proved in Ref. 31, in which Wigner terminology was used. In this reference it was also shown that the focal lengths of the three lenses are related to the desired fractional order as

$$L_{p_1} = \frac{f_1}{\tan\frac{\phi}{2} + 1}, \tag{4.57}$$

$$L_{p_2} = \frac{f_1}{\sin\phi + 2}, \tag{4.58}$$

$$L_{p_3} = L_{p_1}, \tag{4.59}$$

where f_1 is a scaling constant of the FRT that exists in the physical coordinates $\{x_r = [x_{\mathrm{ph}}/(\lambda f_1)^{1/2}]\}$ and ϕ is related to the fractional order p as $\phi = [(p\pi)/2]$.

Figure 4.8 illustrates the optical setup used to obtain the LFRT. In this setup three filter plates are drawn. The input plate is divided into areas; in each area a different fractional order is to be applied. Every area is also multiplied by a quadratic-phase filter (a lens) of $\exp[(-i\pi x^2)/(\lambda L_{p_1})]$. L_{p_1} is calculated according to Eq. (4.57), and the ϕ value in the equation is determined according to the fractional order applied in that specific spatial area

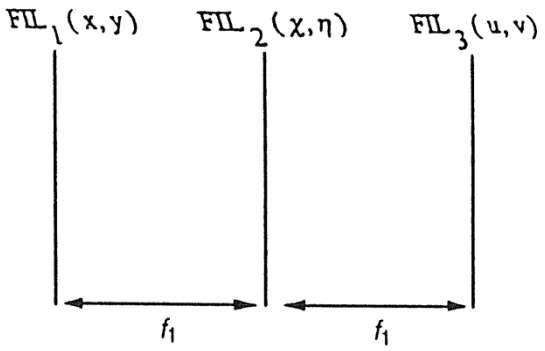

Fig. 4.8. Optical setup for obtaining the LFRT.

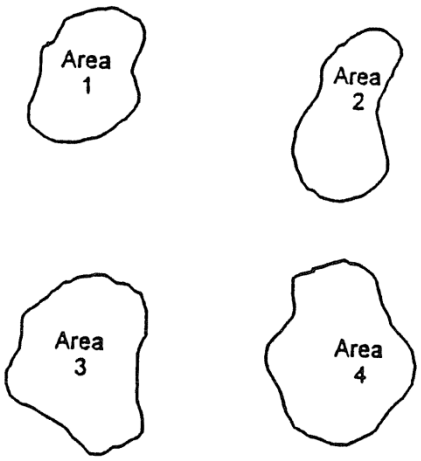

Fig. 4.9. Separation of the different areas $A_i(x, y)$ to the different channels.

$A_i(x, y)$. Hence the input mask plate is

$$\mathrm{FIL}_1(x, y) = \sum_i A_i(x, y) R_{i_1}(x, y) \mathrm{LENS}_1(p_i), \tag{4.60}$$

where $R_{i_1}(x, y)$ is the Ronchi grating and $\mathrm{LENS}_1(p_i)$ is the lens suitable for the specific spatial area according to Eq. (4.57). Note that the mask is plotted as a single diffractive optical element. The Ronchi grating $R_{i_1}(x, y)$ is added to the mask in order to obtain spatial separation between the different areas that are about to be processed by the different FRT orders. A full spatial separation is needed so that information on the different spatial areas will not be mixed. The Ronchi grating separates the different areas into different channels by aiming the information of each area to a different spatial region. One controls the amount of separation between the different channels by changing the direction and the rate of the lines in the grating $R_{i_1}(x, y)$. Note that the spatial separation will be obtained after the free-space propagation.

When the light hits the second mask $\mathrm{FIL}_2(\xi, \eta)$, the information of the different areas $A_i(x, y)$ is already spatially separated into different channels, as illustrated in Fig. 4.9.

Thus the function of the second mask is

$$\mathrm{FIL}_2(\xi, \eta) = R_{i_2}(\xi, \eta) \mathrm{LENS}_2(p_i) \tag{4.61}$$

per each spatial channel.

$R_{i_2}(\xi, \eta)$ is another Ronchi grating that is supposed to correct the undesirable linear-phase factor introduced by the first Ronchi grating (exactly as was done in the multifacet method [32]). The term $\mathrm{LENS}_2(p_i)$ indicates the lens that is suitable for a specific channel and calculated according to Eq. (4.58).

After additional free-space propagation, the last mask $\mathrm{FIL}_3(u, v)$ is placed. This mask consists of a lens calculated according to Eq. (4.59) for each spatial channel (each channel corresponds to a different fractional order). At the output plane, the FRT of each order is obtained in different spatial locations.

4.5.2 General applications

The applications of the suggested transformation could be significant in deterministic as well as in statistic signal processing.

A reconstruction of a FRT processor that can deal with several FRT orders simultaneously expands the application list of the FRT. The FRT by itself is an optimal tool for filtering chirp noise because in the FRT domain this type of noise becomes a delta function that can be easily filtered [12]. However, an object with chirp noise that, in different locations, appears with different densities cannot be handled effectively by a fixed FRT order. Another important application of a varying FRT's order processor relates to an application in which different amounts of shift variance are needed in different regions of the object. For example, an envelope for which one may want to detect the stamp with high shift variance (fractional order close to 0) and the zip code with low shift variance (fractional order close to 1) needs a processor with more than one FRT order.

Note that the alternative solution of splitting the input into several channels, while each channel handles one specific FRT order, is expensive if a space–bandwidth product or intensity limits exist for the system. Also, if after the processing one wants to compose back the image, it becomes much more complicated when one is dealing with multichannel systems. Furthermore, the option of using a cascade filter (which for some applications might be effective) usually does not have good results. Figure 4.10 illustrates such a case; it presents a Wigner chart. The signal is plotted as the filled shapes and the noise is represented by the unfilled shapes. A cascade application of a FRT will cause a rotation of the total chart

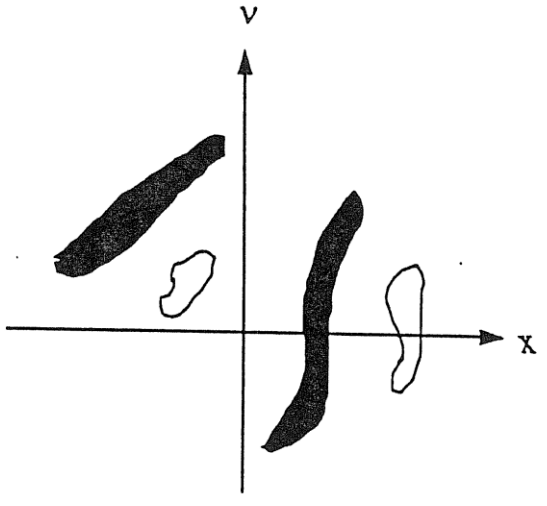

Fig. 4.10. Wigner chart of a case in which the LFRT is useful.

[14]. For any possible rotation, no separation between all parts of the signal and the noise is possible. However, if a LFRT is applied, the separation may be achieved. The optimal method for this case is to apply a different-order FRT for the regions $x < 0$ and $x > 0$. For the region $x < 0$ one should rotate the Wigner chart at an angle that is required for separation between the signal and the noise in this region. For $x > 0$ a different rotating angle should be applied in order to perform the separation. After the filtering of the noise, a perfect reconstruction of the signal will be obtained.

An additional possible application of the LFRT is to repeat the derivation done in Section 2 for the FC performance optimization. In those derivations it was shown that the optimal filter for the FC case is object dependent and that the fractional order p can optimize performance criteria as the SNR or the PCE ratio. Here we have another degree of freedom, which is the spatial dependence of p: $p(x, y)$. Thus, by the design of an optimal spatially dependent filter, the performances might be improved, as p is no longer a constant, but a function.

4.5.3 Application for pattern recognition

The most common case in which different spatial shift-variant processing is required relates to fingerprint recognition [21]. The fingerprint is a pattern whose spatial variance is changed with the spatial location. Its central region is more or less constant, whereas the outer one is changed from instant to instant as one never presses his or her finger with equal force. Thus, in order to recognize or reconstruct those prints, a processor whose spatial shift variance is changed is required. Because of the physical construction of the filter, a small shift invariance is needed in the center, but in the outer regions of the print, an increasing shift invariance is required. In this practical case a LFRT processor should be helpful, because an efficient recognition of the fingerprints can be applicable, for example, in safety lockers or in gaining admittance to permission-restricted entrances.

4.5.3.1 Computer simulations

In our computer simulations two fingerprints of 256 × 256 pixels were taken from the same finger of the same person. Both fingerprints are illustrated in Figs. 4.11 and 4.12.

One of the prints was taken as the reference object while the other was used as the testing input. As the first stage in our simulated experiment, a conventional Fourier analysis was done. The input was Fourier transformed, multiplied by the conjugate of the Fourier transform of the reference object, and finally inverse Fourier transformed. The central line profile of the obtained correlation peak is shown in Fig. 4.13.

Note that, in order to obtain fair performance comparisons in each simulation, the MF was normalized by the energy of the reference pattern. As one can note, the quality of the correlation peak is not very good. For the second stage, a FRT analysis was done. The input pattern was fractionally Fourier transformed by the order of p, multiplied by the conjugate of the fractionally Fourier-transformed (also by fractional order of p) reference object. The multiplication was eventually fractionally Fourier transformed by the order of -1 (an inverse Fourier transform). This is according to the definition of the optimal FC that is given in Ref. 9. This procedure was done for different fractional orders. The fractional order that was optimal according to the correlation peak form was found to be $p = 0.9$. Figure 4.14 illustrates the central line profile of the output correlation peak obtained for $p = 0.9$.

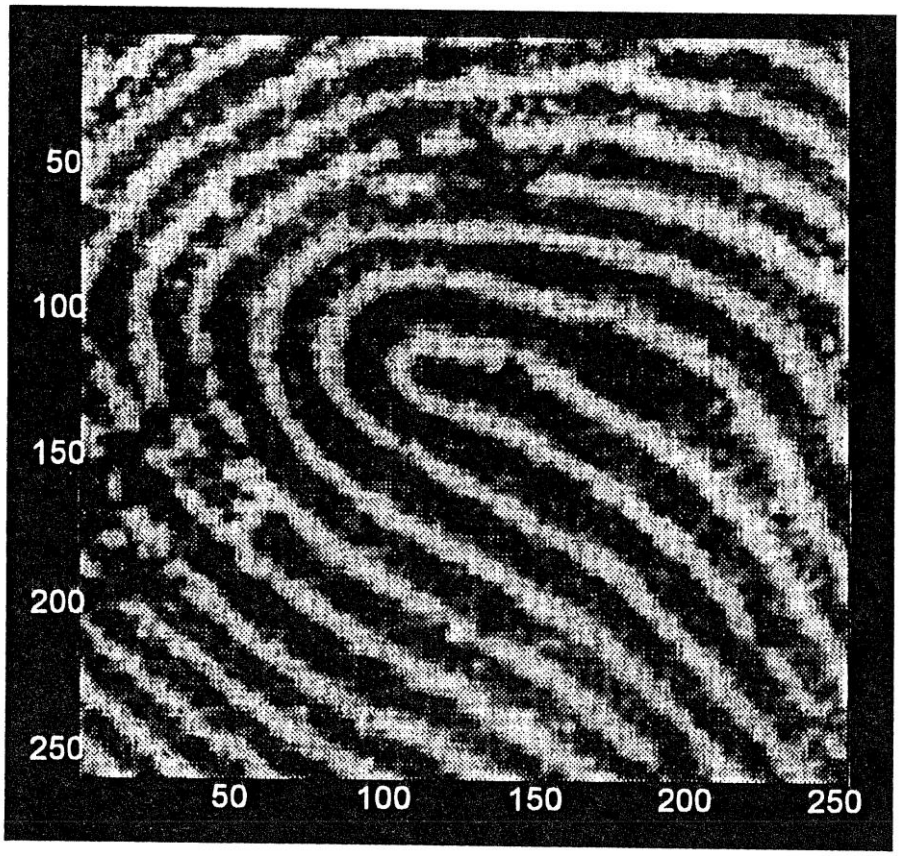

Fig. 4.11. Fingerprint used as the reference object.

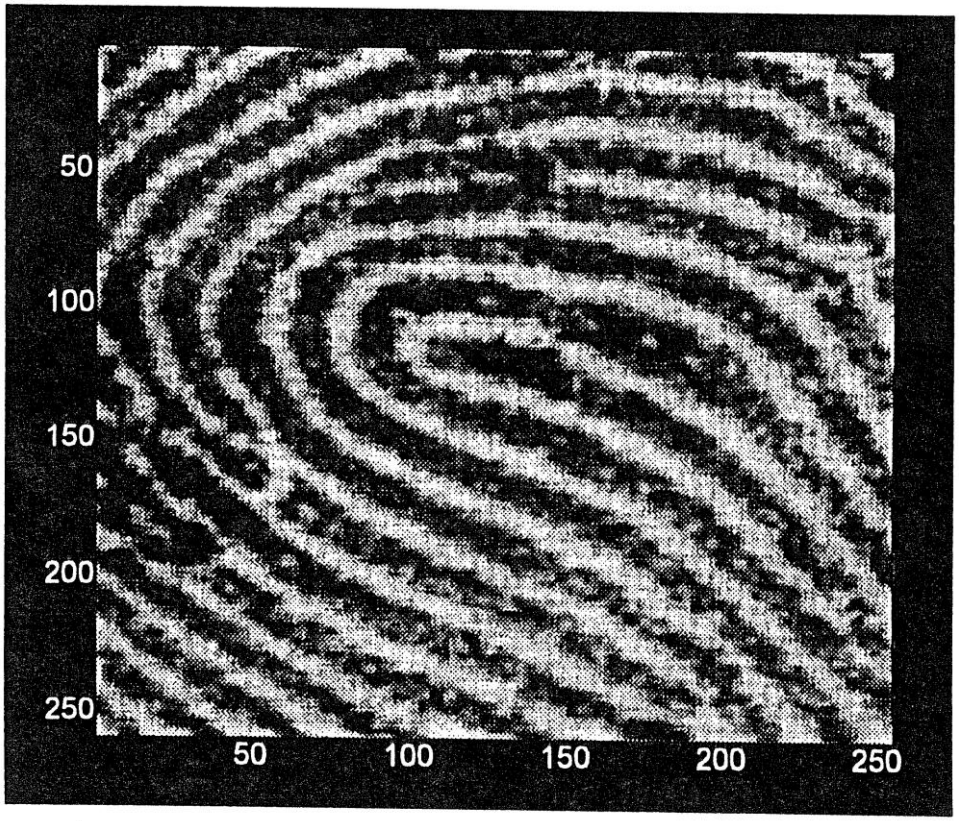

Fig. 4.12. Fingerprint used as the input object.

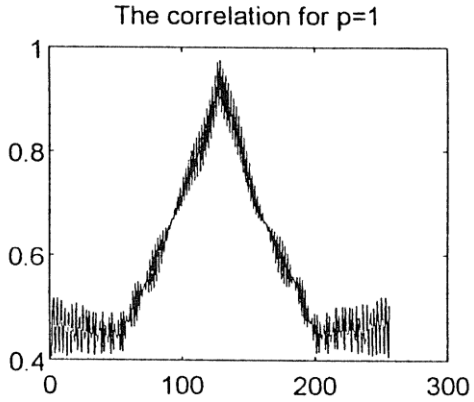

Fig. 4.13. Central line profile of the correlation peak when Fourier processing is used.

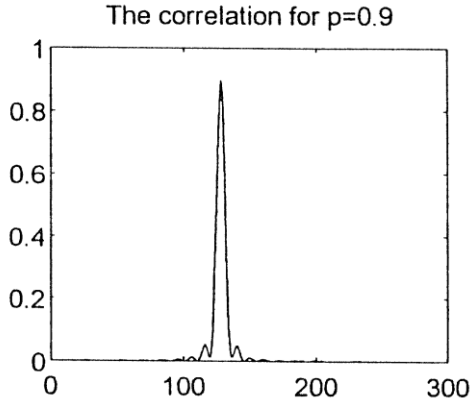

Fig. 4.14. Central line profile of the output correlation when FRT processing of $p = 0.9$ is used.

As one can note, the peak is much narrower than that of Fig. 4.13. Thus, for the fingerprint case, partial space-variant filtering obtains a much better performance than a regular Fourier analysis. For the third stage, a LFRT was applied. As mentioned above, the inner area of the print is less space variant than the outer area. Thus the fractional order for the inner area should be smaller than that for the outer area. The processing filter should be more space invariant at its outer region than at its inner ones. We divided the processing zone into two areas: the inner area, which was defined for the pixels $64 < x < 192$, $64 < y < 192$, and the outer area, which was all the rest. After some computer investigation we found that the optimal fractional order for the inner area is $p = 0.86$ and for the outer one is $p = 0.94$. Thus the constructed processor performed a FRT of $p = 0.86$ in the inner area and a FRT of $p = 0.94$ in outer one. The processor may be optically implemented as illustrated in Ref. 20 and in section 4.5.1.

The LFRT processor of Ref. 20 is multichannel. The two processing areas are separated by reference gratings. A suitable correlation peak is obtained in each processing channel. The processing over the inner area contains the performance of a FRT of $p = 0.86$ over the inner area, multiplying it by the inner area of the reference object that is fractionally Fourier transformed with $p = 0.86$ and obtaining a FRT of $p = -1$ over the result. The processing over the outer area is exactly the same procedure, but is performed with the fractional order of $p = 0.94$ instead of 0.86. The profile of the central line in the obtained correlation peak is shown in Fig. 4.15. Figure 4.16 illustrates the same but for the outer region.

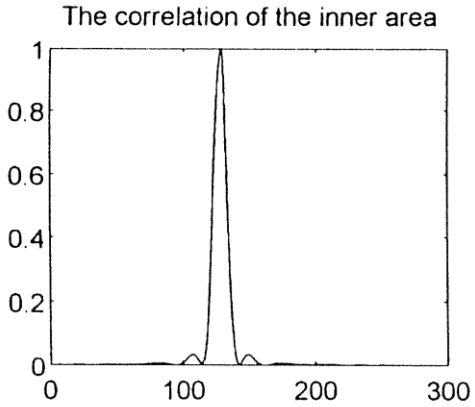

Fig. 4.15. Central line profile of the correlation peak obtained for the inner area of LFRT processing.

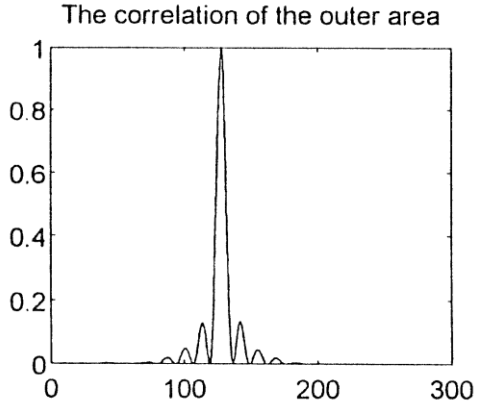

Fig. 4.16. Central line profile of the correlation peak obtained for the outer area of LFRT processing.

As one can note, both peaks are very sharp and narrow. The obtained peaks are ~10% higher than the peaks of Fig. 4.14 or Fig. 4.13. Thus the performances of the LFRT are better compared with those of the conventional Fourier processor or the optimal uniform FRT processor. A complete LFRT would combine the two detected images to gain even more discrimination.

4.6 Anamorphic fractional Fourier transform for pattern recognition

4.6.1 Anamorphic fractional Fourier transform

The FRT concept can be extended to the anamorphic case [22, 23]. This modification permits the use of different fractional orders for two orthogonal axes of a two-dimensional image. The main potential of the anamorphic transform is its possibility of achieving different amounts of shift variance in the two different axes. A clear example for its advantage occurs when shift-invariant detection of objects along a row is needed. However, in the direction perpendicular to the row, there is no need to keep the shift-invariance property. Depending on the characteristics of the object to be detected, the decrease of shift invariance may result in a gain in the performance of the correlator, mainly in peak sharpness and the SNR [9, 33]. In addition, in special cases, the shift variance can help in locating the object. The

detection peak will be produced only when the input object lies along the line where the shift invariance is kept.

The anamorphic FRT is defined as [34]

$$F^{p_x,p_y}(x',\ y') = \int_{-\infty}^{\infty}\int_{-\infty}^{\infty} f(x, y)\exp\left[i\pi\left(\frac{x^2 + x'^2}{T_x} + \frac{y^2 + y'^2}{T_y}\right)\right.$$
$$\left. - 2i\pi\left(\frac{xx'}{S_x} + \frac{yy'}{S_y}\right)\right]\mathrm{d}x\,\mathrm{d}y, \tag{4.62}$$

where

$$T_x = \lambda f_{1x}\tan\phi_x, \qquad S_x = \lambda f_{1x}\sin\phi_x, \qquad \phi_x = p_x(\pi/2),$$
$$T_y = \lambda f_{1y}\tan\phi_y \qquad S_y = \lambda f_{1y}\sin\phi_y, \qquad \phi_y = p_y(\pi/2) \tag{4.63}$$

where the subscripts x and y indicate the horizontal and the vertical directions of the system, respectively. Because here we are dealing with physical implementation as well, we use the physical coordinate set. The additivity property of the FRT allows us to implement the anamorphic FRT by cascading an amorphic setup, which performs the FRT with the order that is the lower between p_x and p_y and an anamorphic system that obtains a FRT in one axis and imaging in the other one [23]. Other setups providing a higher compactness or flexibility have also been proposed [22, 23].

An alternative approach for obtaining the anamorphic FRT is based on the setup described in Ref. 35. Instead of preparing a full setup containing two lenses and free space propagation, one illuminates the object with a converging beam. The convergence-phase factor, multiplying the object, may be changed by the displacement of the object along the optical axis. The matching between the distance object–filter and the convergence beam phase may produce any desired order and scaling factor for the FRT. This fact makes the last approach more convenient for the experimenter, as the exact sizes of the transparencies are often not precisely determined. Note that the FRT obtained in this method is inexact. It does not have the final quadratic-phase factor, and thus the correlation plane will be displaced along the optical axis. In the case of an anamorphic FRT the convergence of the beam at the output of the filter plane will be different in the two main axes. In order to focus the correlation, an anamorphic system will be needed.

The setup for performing the anamorphic fractional correlation is shown in Fig. 4.17.

The adjustment of distances a_x and a_y determines the proper order for the FRT. The scale factor of the FRT is variable, as a parameter independent of the order. For practical reasons one should try to reduce the number of cylindrical lenses in the constructed optical setup. In the chosen configuration, only three cylindrical lenses and one spherical lens are used.

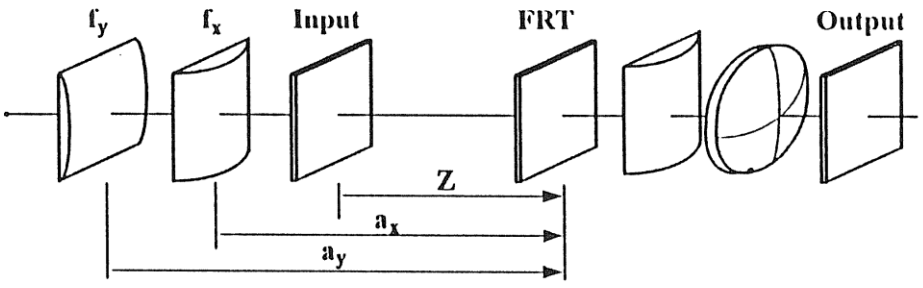

Fig. 4.17. Experimental setup for obtaining the anamorphic fractional correlation.

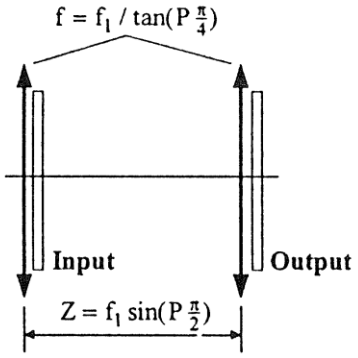

Fig. 4.18. Optical setup for performing a FRT operation.

The price to be paid for this simplification is the aspect ratio of the FRT (quotient between the x and that y scale ratios), which cannot be adjusted. Inserting an additional anamorphic image forming system (which provides different magnifications in both axes) stretches the image of the FRT plane and corrects the problem. The output of this imaging system is then taken as the input for the inverse-transforming subsystem. This additional complexity can be avoided in most practical cases. As shown in Figs. 4.17 and 4.18, because the Z distance is equal for both axes, one may write the following:

$$Z = Z_x = f_{1x} \sin\frac{p_x\pi}{2} = Z_y = f_{1y} \sin\frac{p_y\pi}{2}. \tag{4.64}$$

Thus the aspect ratio (AR) between the two axes is

$$\mathrm{AR} = \frac{f_{1x}}{f_{1y}} = \frac{\sin\dfrac{p_y\pi}{2}}{\sin\dfrac{p_x\pi}{2}}. \tag{4.65}$$

4.6.2 Multiple fractional-Fourier-transform filters

One of the motivations of the anamorphic FRT approach is to design a composite filter that is able to recognize object A or a certain deformation of this object in region $\mathcal{A}$ and object B or a certain deformation of it in region $\mathcal{B}$. In order to obtain these capabilities, an anamorphic FC is used.

To implement the demands, we place object A in region $\mathcal{A}$, which is assumed to be in the upper part of the input scene. If a FRT of 0.5, for example, is performed over this input over the y axis, the obtained fractional spectrum will be concentrated mainly in the upper region of the output plane (region $\mathcal{A}$). Because the fractional order of 0.5 determines a transformation that is only partially shift invariant, shifting the input object therefore causes a shift of the fractional spectrum. This does not occur in the conventional Fourier transform ($p = 1$), in which the shift of the input object is expressed by only a linear-phase factor in the spectral plane. The same happens if object B is placed in the lower region of the input scene (region $\mathcal{B}$). This results in a fractional spectrum that is concentrated mainly in the lower part of the fractional spectrum. Thus a simple summation of the fractional spectra of A and B will create a joint spectrum basically without overlapping between each one of the spectra (A and B) individually. The obtained filter is able to recognize only object A in region $\mathcal{A}$ of the input scene (upper part) and only object B in region $\mathcal{B}$ (lower part).

Assuming that along axis x one wishes to obtain full shift invariance, i.e., when object A is located in region $\mathcal{A}$, object A can move along the x axis and yet be recognized, and the same property should be ensured for object B. Thus a FRT with a fractional order of 1 (conventional Fourier transform) over the x-direction should be performed.

We now summarize the procedure for preparing the filter for a certain example. We denote by p_x the fractional order performed in the x axis and by p_y the fractional order in the y axis. Object A is shifted to the center of region $\mathcal{A}$ and an anamorphic FRT is calculated with the fractional orders of $p_x = 1$ and $p_y = 0.5$. The complex conjugate of this distribution is taken. Now this filter itself will detect the presence of object A at the center of region $\mathcal{A}$ by producing a correlation peak located in the center of the output plane. Because it is more convenient if the peak is produced over the object and not in the center of the output, the filter is multiplied by a linear-phase factor that deviates the correlation peak to the object's location. This linear-phase factor is calculated according to the distance between the center of the input image and the position where the target has been displaced in the first step of the filter preparation (the center of region $\mathcal{A}$). The same process is repeated for object B, with the corresponding displacement to the center of region $\mathcal{B}$. The two distributions obtained in this way are added to construct the final filter. The resulting filter is placed in the appropriate fractional Fourier domain in the anamorphic correlator.

If, instead of detecting object A in region $\mathcal{A}$ and object B in region $\mathcal{B}$, one prefers to detect a certain deformation of object A in region $\mathcal{A}$ and a different deformation of object B in region $\mathcal{B}$, the same approach can be applied. Let us assume that a one-dimensional (1-D) x-direction scaling-invariance property of object A is required to be detected in region $\mathcal{A}$ and a 1-D y-direction scaling invariance of object B is required to be detected in region $\mathcal{B}$. One way of obtaining a 1-D scale invariance is to use the logarithmic harmonic decomposition [36]. Thus here object A was decomposed to the proper logarithmic harmonic (x scaling invariant), and the harmonic was shifted to the center of region $\mathcal{A}$. In the same manner, object B was decomposed to the proper logarithmic harmonic (y scaling invariant), and the harmonic was shifted to the center of region $\mathcal{B}$. Then a FRT with the fractional orders of $p_x = 1$, $p_y = 0.5$ is performed over the sum, and a complex conjugate of this function is obtained. The resultant filter is placed in the fractional domain of the anamorphic FC. Note that, when this approach is used, any invariant property can be detected in region $\mathcal{A}$ or $\mathcal{B}$ if the proper harmonic decompositions are used in each region.

4.6.3 Optical implementation

In the FRT processor the scale of a filter's distribution is crucial for obtaining the desired results. In a case in which the input object is recorded on photographic film and the filter is generated by a computer, the scales can be matched during the recording process. However, this requires high accuracy. Moreover, if instead of a computer-generated hologram, spatial light modulators are used for either the input transparency or the filter, the scale cannot be controlled. Special difficulties appear when the sizes of input and output do not match. A way to overcome this problem is to use an adjustable anamorphic FRT correlator [35]. It is based on the setup depicted in Fig. 4.18, in which the order can be varied by a change in the focal length of the lenses and the distance between input and output. Illuminating the input transparency with a nonparallel beam and displacing the object along the optical axis vary the convergence of the beam that illuminates the input. This is fully equivalent to changing the focal length of the first lens in the setup of Fig. 4.18. The separation between

the input and the output must be varied accordingly so that the condition for being a FRT of the desired order is fulfilled. The second lens is removed from the setup. The result is a fractional transform with a variable scale, but with an additional quadratic-phase factor in the output plane. Because in a FC the anamorphic transformer is only the first stage of the complete correlator, the quadratic-phase factor will change only the position of the output correlation plane.

4.6.4 Results

4.6.4.1 Computer simulations

Several computer simulations were performed to demonstrate the performances of the proposed filter. For those simulations the input image illustrated in Fig. 4.19 was used.

The constructed filter is supposed to recognize an F-18 airplane in the upper part of the input and a Tornado airplane in the lower part. As mentioned above, for the construction of the filter, the F-18 airplane was shifted to the center of the upper part of the image and the Tornado was shifted to the center of the lower part. The above-outlined procedure was followed to obtain a filter with the fractional orders of $p_x = 1$, $p_y = 0.5$. The chosen fractional orders caused the filter to be fully shift invariant in the x direction and also to allow a small amount of shift invariance in the y axis. In the input scene illustrated in Fig. 4.19, the y positions of the centers of the F-18 airplanes in the upper part and the y positions of the Tornado airplanes' centers in the lower part were separated by few pixels. Figure 4.20 is the obtained output plane. One can note good correlation peaks that indicate the existence of the F-18 in the upper part and the Tornado in the lower part.

The possibility of recognizing different deformation properties in different parts of the image is demonstrated in Fig. 4.21.

In this case the purpose was to obtain an x scale-invariant recognition of F-18 airplanes in the upper part of the scene and a y scale-invariant recognition of the same target in the lower part. For the construction of the filter, an x scale-invariant logarithmic harmonic of the F-18 was calculated and shifted to the center of the upper region of the image. Then a

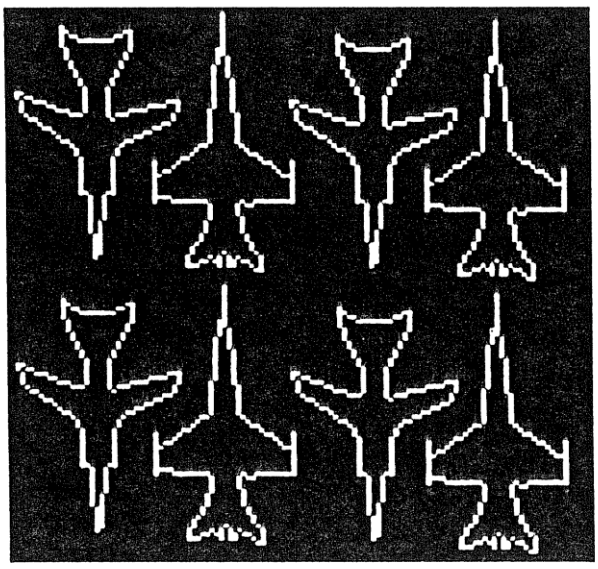

Fig. 4.19. Input image used for computer simulations and optical experiments.

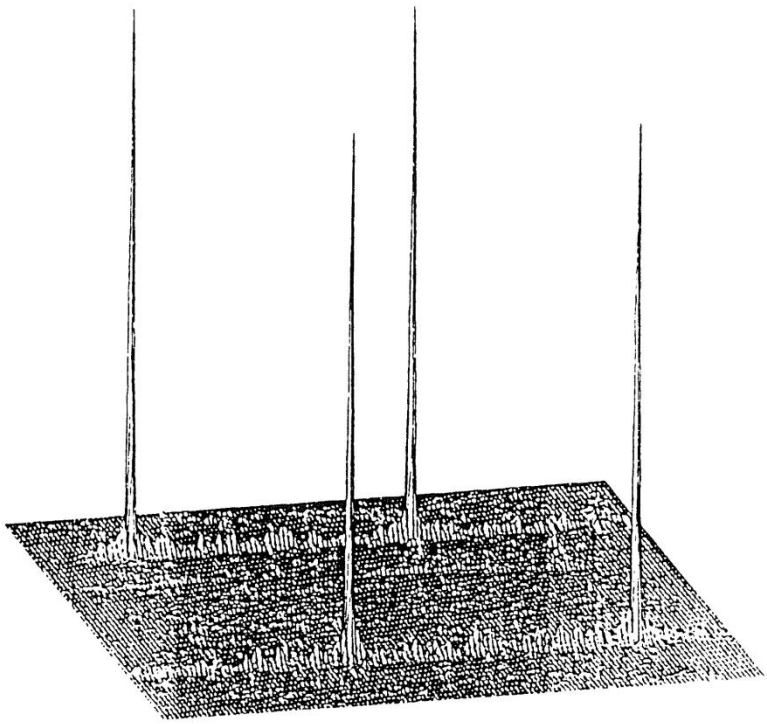

Fig. 4.20. Numerical calculation of the correlation that shows detection of the F-18 target in the upper part of the image and the Tornado in the lower part.

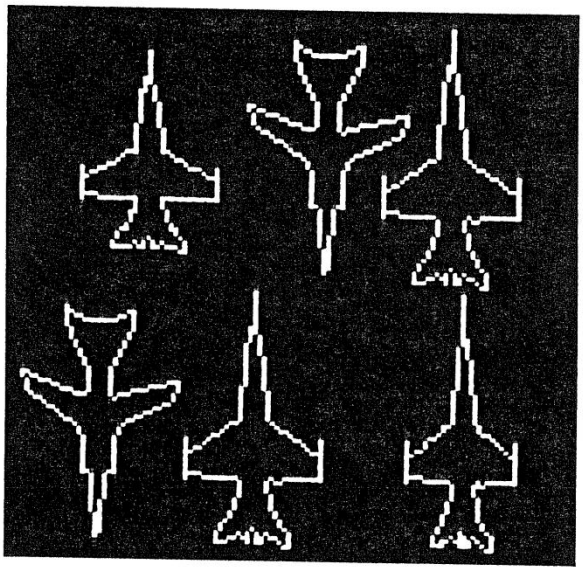

Fig. 4.21. Input image used for computer simulations.

y scale-invariant logarithmic harmonic of the F-18 was calculated and shifted to the center of the lower region of the image. The above-outlined procedure was performed to obtain a filter with $p_x = 1$, $p_y = 0.5$. Successful recognition is demonstrated by the distinct correlation peaks of Fig. 4.22.

A threshold of 35% of the maximum intensity value is enough to detect the true target peaks from the peaks that correspond to other objects and from the background.

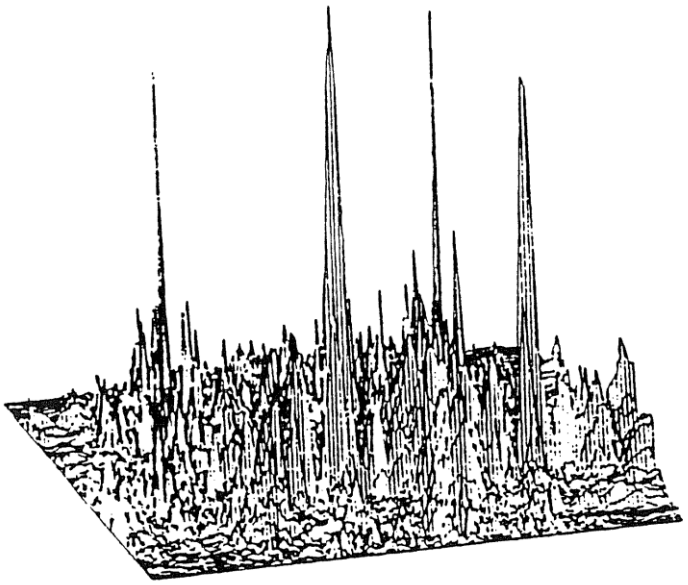

Fig. 4.22. Numerical calculation of the correlation that shows detection of the F-18 target with invariance to a 1-D scale in two axes.

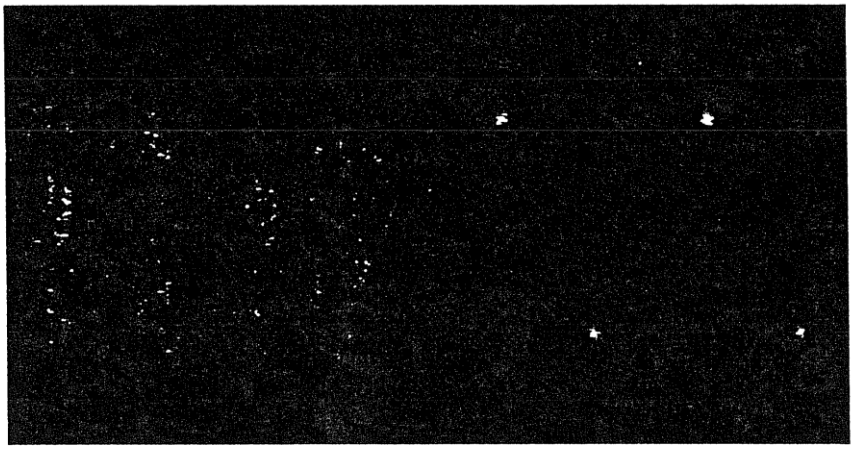

Fig. 4.23. Experimental results for a multiple anamorphic FRT correlation with the image in Fig. 4.19.

4.6.4.2 Optical results

In order to test the performance of the suggested approach experimentally, a binary computer-generated mask was plotted. Then it was reduced by 20% with a high-resolution camera. The hologram was a 128 × 128 pixel Lohmann encoding mask [37]. The input scene size was 4.2 × 4.2 mm, and the filter size was 8.5 × 12 mm. This aspect ratio between the axes was calculated according to Eq. (4.65) [AR = $\sin(0.5\pi/2)/\sin(\pi/2) = 8.5/12$]. At the output plane, a CCD camera connected with a Matrox image LC framegrabber was used in order to grab the correlator output. The input scene is illustrated in Fig. 4.19. The experimentally obtained output is shown in Fig. 4.23.

These pictures show the intensity at the output correlation plane. The experimentally obtained results appearing in the first diffraction order match with the computer simulations illustrated in Fig. 4.20. In order to adjust the system a special plate was used, as explained in Refs. 24 and 35.

4.7 Fractional joint transform correlator

The JTC configuration is based on the simultaneous presentation of two patterns at the input plane, each laterally shifted from the center of the axis. Thus such an approach does not require the generation of a complex filter and aligning it with high accuracy in the Fourier plane. As Fig. 4.24 shows, a schematic configuration of the JTC contains a 4-f setup that at its Fourier plane includes a square-law converter device (a device that converts field distribution to amplitude distribution).

The output first diffraction orders of such a method are the correlation between the two input patterns. Several approaches for implementing the square-law conversion have been suggested, such as photofilm [3], a spatial light modulator [38], and liquid-crystal light valves [39]. When the shift invariance of the input plane is not important, a fractional JTC configuration may be used [25]. This configuration is first analyzed and then optically implemented in this section. The advantages of such a configuration in the optical pattern recognition field are similar to the advantages of the conventional JTC approach, but, in addition, the amount of the shift invariance can be controlled.

Because the mathematical analysis done in this section relies on the Wigner distribution function (WDF), a brief background is given [25, 40].

4.7.1 Wigner distribution function

The WDF of a signal $U(x)$ is defined as

$$W(x, \nu) = \int U(x + x'/2)U^*(x - x'/2)\exp(-2\pi i \nu x')\,\mathrm{d}x', \tag{4.66}$$

or alternatively, with $\tilde{U}(\nu)$, the spectrum of $U(x)$ [$\tilde{U}(\nu) = \int U(x)\exp(-2\pi i \nu x)\,\mathrm{d}x$]:

$$W(x, \nu) = \int \tilde{U}(\nu + \nu'/2)\tilde{U}^*(\nu - \nu'/2)\exp(+2\pi i \nu' x)\,\mathrm{d}\nu'. \tag{4.67}$$

U may be reconstructed out of W, apart from a constant phase factor:

$$\int W(x/2, \nu)\exp(2\pi i \nu x)\,\mathrm{d}\nu = U(x)U^*(0). \tag{4.68}$$

The signal intensity $|U(x)|^2$ and the power spectrum $|\tilde{U}(\nu)|^2$ can be obtained from W by two orthogonal projection integrals:

$$\int W(x, \nu)\,\mathrm{d}\nu = |U(x)|^2, \tag{4.69}$$

$$\int W(x, \nu)\,\mathrm{d}x = |\tilde{U}(\nu)|^2. \tag{4.70}$$

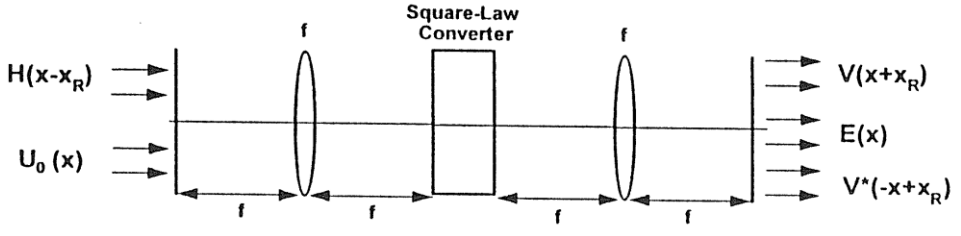

Fig. 4.24. Schematic optical setup for performing the joint transform correlation.

Shifting of the WDF occurs in the (x, ν) domain if the signal $U(x)$ is shifted and is illuminated by a tilted plane wave, $\exp(2\pi i \bar{\nu} x)$:

$$U(x) \longrightarrow U(x - \bar{x}) \exp(2\pi i \bar{\nu} x), \tag{4.71}$$

$$W(x, \nu) \longrightarrow W(x - \bar{x};\ \nu - \bar{\nu}). \tag{4.72}$$

Note that, as illustrated in Ref. 14, the FRT operation is defined as what occurs to U_0 while the WDF is rotated by an angle $\phi = p\pi/2$:

$$U_0(x) \longrightarrow U_p(x), \tag{4.73}$$

$$W_0(x, \nu) \longrightarrow W_0(x \cos\phi - \nu \sin\phi,\ \nu \cos\phi + x \sin\phi) = W_p(x, \nu), \tag{4.74}$$

where $U_p(x)$ is a FRT with the fractional order of p applied over $U_0(x)$, W_0 is the WDF of U_0, and W_p is the WDF of U_p.

4.7.2 Concept of the joint fractional correlator

Based on the FRT operation, we generalize the classical JTC (Fig. 4.25). To do so, the classical Fourier transforms are now replaced by FRT's (Fig. 4.26).

There is a hidden problem in this flow chart. We identify this problem by stepping into the Wigner domain.

Step I:

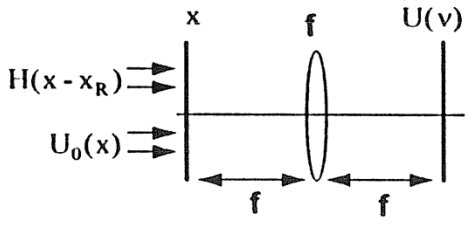

Step II:

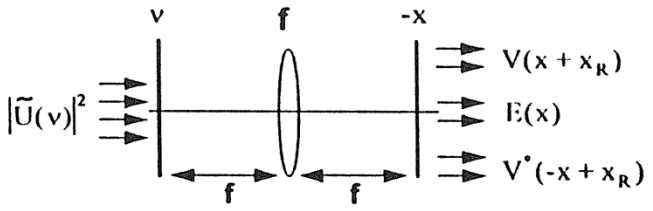

Fig. 4.25. JTC. U_0, input; H, reference signal; $\tilde{U}$, complex amplitude in the Fourier domain; $|\tilde{U}|^2$, transmission of the holographic filter; V, output; E, extraneous term.

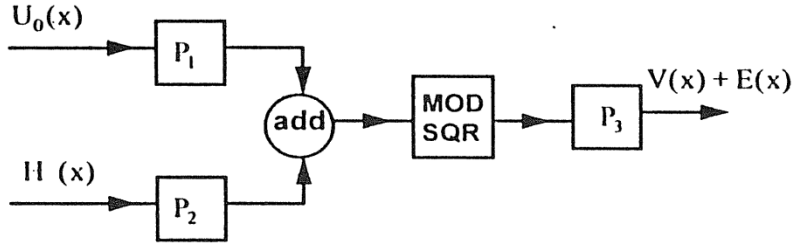

Fig. 4.26. Flow diagram of the joint fractional correlator. MOD SQR, modulus-square.

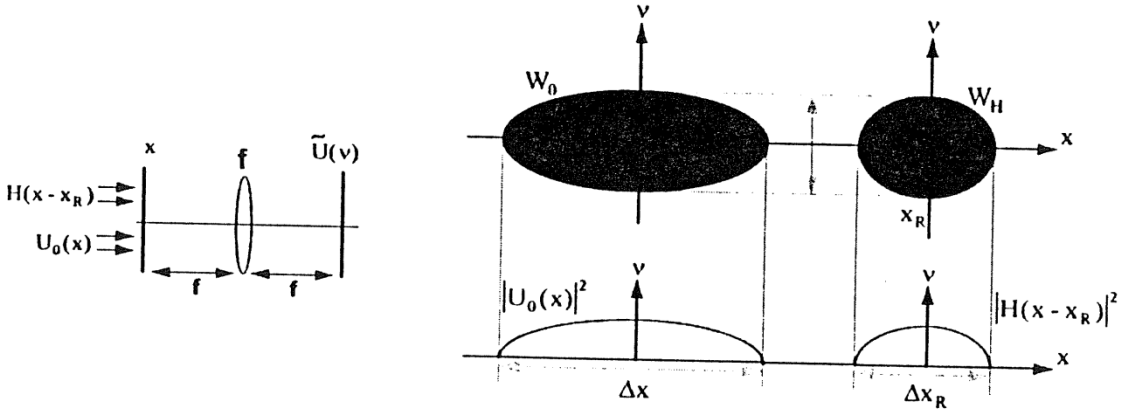

Fig. 4.27. WDF of the input to Fig. 4.25, step I, and the projection of that WDF, which is the input intensity to Fig 4.25, step II.

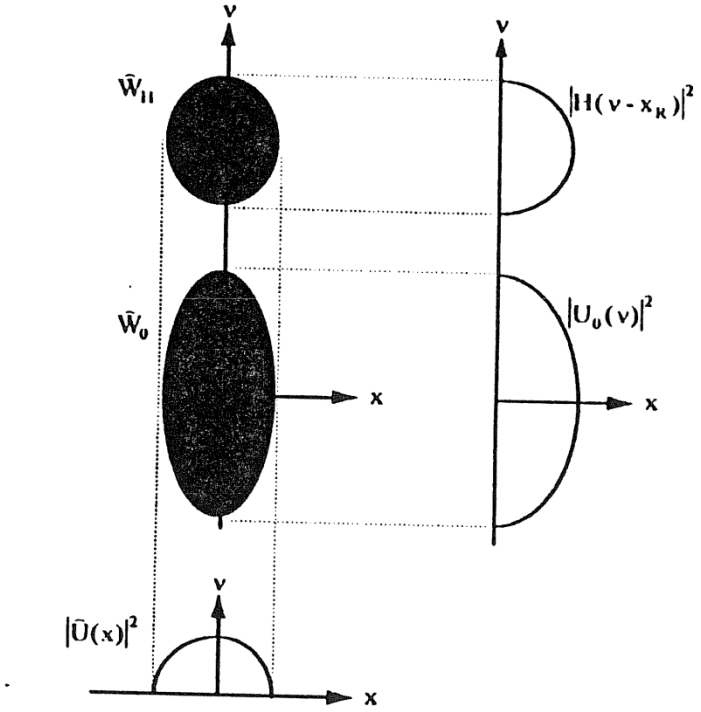

Fig. 4.28. WDF of the output to Fig. 4.25, step I, together with the two projections, intensity (x) and power spectrum (ν).

4.7.3 Removal of the extraneous terms

The need to remove some extraneous terms already occurred in the classical JTC system. However, in the classical JTC case the solution is simple and obvious. Thus we now identify that problem explicitly because it prepares us for solving the more general problem in the joint fractional correlator (JFC) system.

The WDF shown in Fig. 4.27 is the WDF of the two-part signal $U(x) = U_0(x) + H(x - x_R)$ shown in Fig. 4.25, step I.

The Fourier transform in Fig. 4.25, step I, corresponds to a 90° rotation in the Wigner domain (Fig. 4.28). (Note that a space variable x and a frequency variable ν are added in Fig. 4.28 because here we are using the normalized coordinates.)

The WDF contributions of the object and the reference occupy the same X region. Hence the contribution $\tilde{U}_0(x)$ from the object and $\tilde{H}(x)\exp(-2\pi i x x_R)$ from the reference can now interact as parts of the observable WDF projection:

$$\int \tilde{W}(x, \nu)\,\mathrm{d}\nu = |\tilde{U}(x)|^2 = |\tilde{U}_0 + \tilde{H}\exp(-2\pi i x x_R)|^2 = \tilde{U}_0\tilde{H}^*\exp(2\pi i x x_R) + \cdots$$
$$= \tilde{V}(x)\exp(2\pi i x x_R) + \tilde{V}^*(x)\exp(-2\pi i x x_R) + |\tilde{U}_0(x)|^2 + |\tilde{H}(x)|^2, \tag{4.75}$$

where $\tilde{V}(x)$ is the Fourier transform of $V(x)$ (the correlation expression):

$$\tilde{V}(x) = \int \tilde{U}_0(\nu)\tilde{H}^*(\nu)\exp(2\pi i \nu x)\,\mathrm{d}\nu. \tag{4.76}$$

This overlapping between $\tilde{U}_0$ and $\tilde{H}$ is necessary for a successful operation of the JTC. However, the overlapping condition is not sufficient, and in addition it is also required that the wanted term with $\tilde{U}_0\tilde{H}^* = \tilde{V}$ produce an output $V(x + x_R)$ that is laterally separated from the other terms in Eq. (4.75) (Fig. 4.25, step II, right-hand side). In order to comprehend the second request, we consider the WDF of $|\tilde{U}(x)|^2$, which is the input for the second step of the JTC (Fig. 4.25, step II). If the shift x_R of the reference $H(x - x_R)$ is large enough, three separated islands will be created in that WDF. This is illustrated in Fig. 4.29:

$$x_R - (\Delta x_H + \Delta x_0/2) \geq \Delta x_0. \tag{4.77}$$

This condition is well known from holography, in which Δx_H is usually close to zero. In our case the assumption was that $0 \leq \Delta x_H \leq \Delta x_0$.

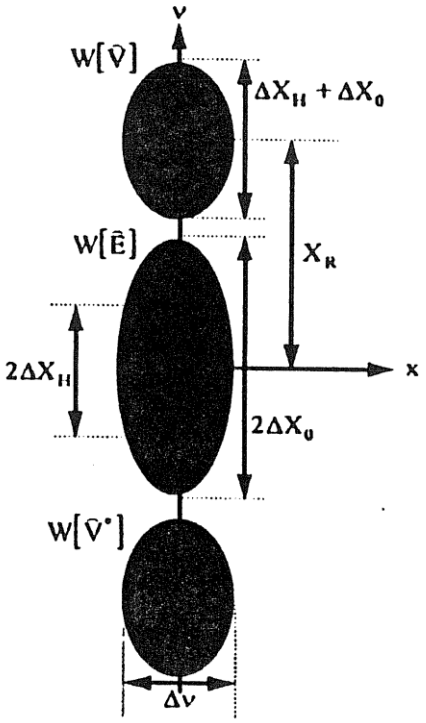

Fig. 4.29. WDF of the intensity output of Fig. 4.25, step I, which is the input for Fig. 4.25, step II.

The second stage of the JTC (Fig. 4.25, step II) is again a Fourier transform that corresponds to a 90° rotation (anticlockwise) of the WDF (see Fig. 4.29). The desired term $V(x + x_R)$ is clearly separated from the extraneous term $E(x)$ and $V^*(-x + x_R)$ if the condition of relation (4.77) is fulfilled. Thus the proper shift of x_R [relation (4.77)] of the reference pattern was necessary and sufficient for the proper JTC operation.

A similar consideration for the JFC yields the fact that the reference $H(x)$ has to be shifted and tilted by proper amounts:

$$H(x) \longrightarrow H(x - x_R)\exp(2\pi i x \nu_R). \tag{4.78}$$

In order to explain this point we translate the front part of the JFC flow chart (Fig. 4.26) into the Wigner domain. The WDF of the centered object $U_0(x)$ is rotated by an angle $\phi_1 = p_1\pi/2$ (Fig. 4.30).

The WDF of the reference signal is shifted at first (Fig. 4.31):

$$W_H(x, \nu) \longrightarrow W_H(x - x_R, \nu - \nu_R). \tag{4.79}$$

Then W_H is subsequently, rotated by an angle of $\phi_2 = p_2\pi/2$. This angle must be such that W_H will end up on the ν axis just above the WDF of U_0 (Fig. 4.32).

Expressing the shift in polar coordinates, we obtain

$$X_R = R\cos(\pi/2 - \phi_2) = R\sin\phi_2, \tag{4.80}$$

$$\nu_R = R\sin(\pi/2 - \phi_2) = R\cos\phi_2. \tag{4.81}$$

This colocation in the x axis is needed to satisfy the condition for letting W_0 and W_H interact when the modulus-square operation of Fig. 4.26 is applied.

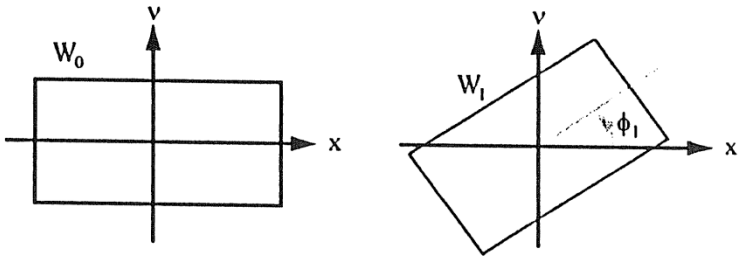

Fig. 4.30. FRT with degree p_1 rotates the WDF of the object by the angle $\phi_1 = p_1(\pi/2)$.

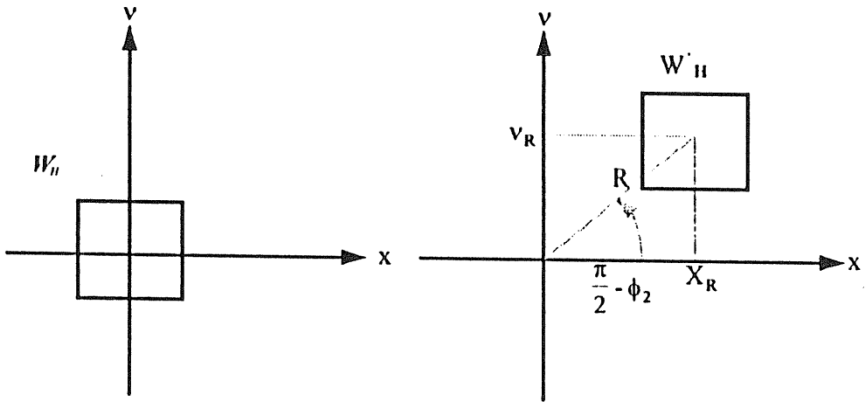

Fig. 4.31. Shift and tilt of the reference signal H cause a shift of the WDF of H. That shift can be expressed by a radius R and an angle $\pi/2 - \phi/2$.

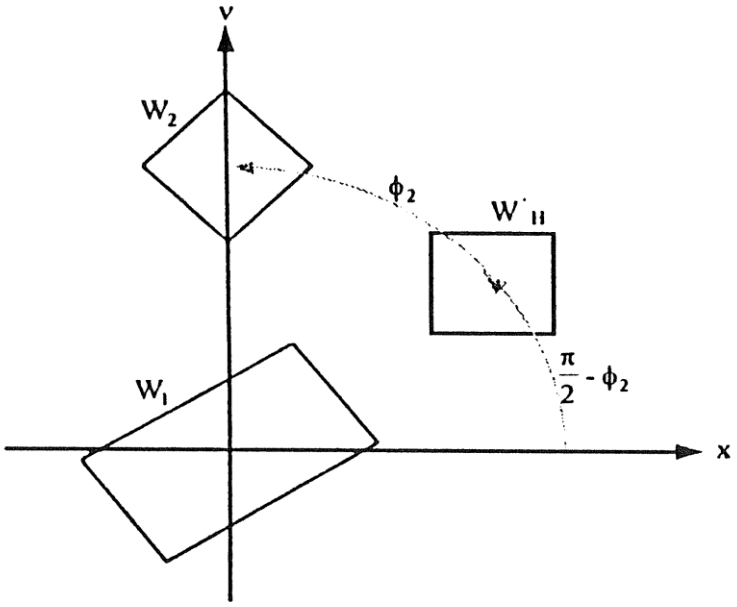

Fig. 4.32. FRT with degree p_2 rotates the WDF of the reference by an angle $\phi_2 = p_2(\pi/2)$, bringing it to the frequency axis on top of the object WDF.

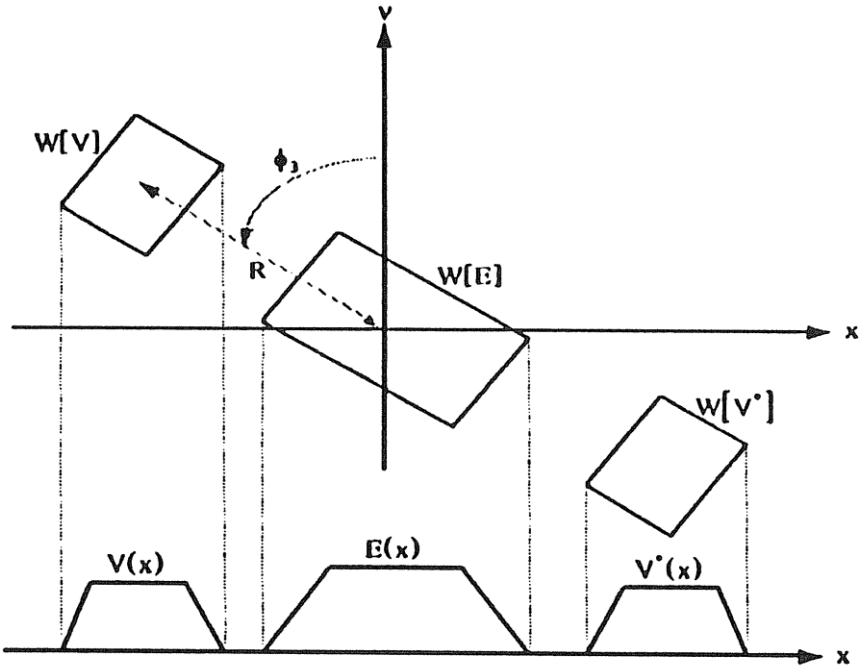

Fig. 4.33. WDF of the JTC output, together with the output intensity distribution.

The obtained WDF of the $|U(x)|^2$ signal consists of three islands, similar to those in Fig. 4.29. But the center-to-center distance between the islands is now R instead of x_R. Note that

$$R^2 = x_R^2 + v_R^2. \tag{4.82}$$

The final step is a rotation of the WDF by an angle $\phi_3 = p_3\pi/2$, as indicated by Fig. 4.26.

The final WDF is shown in Fig. 4.33. In this figure, the radial shift R was sufficiently large to create full separation between the terms $V(x)$ and $E(x)$.

For deriving the condition for R that ensures the separation, one has to calculate the locations of the rectangular WDF islands. The result will be a generalization of the classical condition of separation [relation (4.77)]. However, not only the sizes Δx_0 and Δx_H will appear in the inequality but also the bandwidths $\Delta \nu_0$ and $\Delta \nu_H$, together with cosine and sine factors, involving the three angles ϕ_1, ϕ_2, and ϕ_3. The shortest R will be needed if $\phi_3 = \pi/2$, whereas a small value of ϕ_3 requires large R. If the angle ϕ_2 is small, the R is affected mainly by the tilt ν_R. But with ϕ_2 close to $\pi/2$, the R depends mainly on the shift x_R [as seen from Fig. (4.32) and Eqs. (4.81) and (4.82)].

4.8 Concluding remarks

In this chapter we have attempted to describe the status of the field of fractional correlation that is based on the FRT. The described analysis started by analyzing the performances of the FC compared with those of conventional correlator configurations. Section 4.3 illustrated that the performances are object dependent. For white noise, according to the SNR criterion, the performances of the shift-variant correlator (the FC) are not worse than those of the conventional correlator. For other types of noise, the performances of the FC may be even better (for example, when chirp noise is involved). Then a configuration for obtaining a real-time FC was demonstrated in section 4.4. This configuration is a real-time one because, in order to change the amount of shift variance (the fractional order), one need change only the longitudinal distance of the filter. There is no need to change the distances between the lenses, change their focal length, or recompute the filter. In Section 4.5 the LFRT was defined. This FRT-based transform performs the FRT with different fractional orders in different spatial regions. An optical FC-based on this transform may be constructed. The main advantage of using a FC that is based on the LFRT is when nonstationary noises (with statistical properties that are varied over the space) or special pattern recognition aspects are involved. A pattern recognition example for which such a use is essential was demonstrated for fingerprint recognition. The fingerprint pattern has a spatially varied form. Its central region is more or less constant, whereas the outer region is changed from instant to instant because a person never presses a finger with equal force. Thus, in order to recognize or reconstruct those prints, an LFRT processor whose spatial shift variance is changed with space is required. In Section 4.6 another extension for the FC was illustrated. This time the suggested processor was an anamorphic one. A practical example for which object detection is needed along a row was demonstrated. For cases in which full shift invariance is needed in the one axis and only a limited amount of variance is needed in the other axis, such a processor can be very helpful. The demonstrated example included a case in which a certain first object (or certain deformation property) is needed to be detected in the first region and rejected in the second spatial region and vice versa for the second object (or deformation property) and the second spatial region. Section 4.7 dealt with the JTC configuration applied for the partially shift-variant case. The advantages of the conventional JTC (i.e., it does not require the generation of a complex filter and aligning it with high accuracy in the Fourier plane) were combined with the ability to control the amount of the shift-variance property and implemented optically. In sum, this chapter shows the potential of the FC in various optical signal processing fields. It indicates that the FC adds a degree of freedom that can increase the flexibility of the conventional optical covolver/correlator.

Acknowledgments

The authors acknowledge the fruitful discussions and the generous assistance from A. W. Lohmann and R. G. Dorsch from Erlangen University, C. Ferreira and J. Garcia from the University of Valencia, H. J. Caulfield from Alabama A & M University, Y. Bitran from Tel-Aviv University, and A. Kutay from Bilkent University.

References

[1] A. VanderLugt, "Signal detection by complex spatial filtering," IEEE Trans. Inf. Theory **IT-10**, 139–146 (1964).

[2] A. W. Lohmann and H. W. Werlich, "Incoherent matched filter with Fourier holograms," Appl. Opt. **7**, 561–563 (1968).

[3] C. S. Weaver and J. W. Goodman, "A technique for optically convolving two functions," Appl. Opt. **5**, 1248–1249 (1966).

[4] I. E. Rau, "Detection of differences in real distributions," J. Opt. Soc. Am. **56**, 1490–1494 (1966).

[5] H. O. Bartelt, "Applications of the tandem component: an element with optimum light efficiency," Appl. Opt. **24**, 3811–3816 (1985).

[6] J. R. Leger and S. H. Lee, "Hybrid optical processor for pattern recognition and classification using a generalized set of pattern recognition functions," Appl. Opt. **21**, 274–287 (1982).

[7] J. A. Davis, D. M. Cottrell, N. Nestorovic, and S. M. Highnote, "Space-variant Fresnel-transform optical correlator," Appl. Opt. **31**, 6889–6893 (1992).

[8] G. G. Mu, X. M. Wang, and Z. Q. Wang, "A new type of holographic encoding filter for correlation: a lensless intensity correlator," in *International Conference on Holographic Applications*, J. Ke and R. J. Pryputniewicz, eds., Proc. SPIE **673**, 546–549 (1986).

[9] D. Mendlovic, H. M. Ozaktas, and A. W. Lohmann, "Fractional correlation," Appl. Opt. **34**, 303–309 (1995).

[10] D. Mendlovic, Y. Bitran, R. G. Dorsch, and A. W. Lohmann, "Fractional correlation: experimental results," Appl. Opt. **34**, 1329–1335 (1995).

[11] D. Mendlovic and H. M. Ozaktas, "Fractional Fourier transformations and their optical implementation: part I," J. Opt. Soc. Am. A **10**, 1875–1881 (1993).

[12] R. G. Dorsch, A. W. Lohmann, Y. Bitran, D. Mendlovic, and H. M. Ozaktas, "Chirp filtering in the fractional Fourier domain," Appl. Opt. **33**, 7599–7602 (1994).

[13] H. M. Ozaktas, B. Barshan, D. Mendlovic, and L. Onural, "Convolution, filtering, and multiplexing in fractional Fourier domain and their relation to chirp and wavelet transforms," J. Opt. Soc. Am. A **11**, 547–559 (1994).

[14] A. W. Lohmann, "Image rotation, Wigner rotation, and the fractional Fourier-transform," J. Opt. Soc. Am. A **10**, 2181–2186 (1993).

[15] D. Mendlovic, M. Ozaktas, and A. W. Lohmann, "Graded-index fibers, Wigner-distribution functions, and the fractional Fourier-transform," Appl. Opt. **33**, 6188–6193 (1994).

[16] H. L. Van Trees, *Detection, Estimation and Modulation Theory, Part I* (Wiley, New York, 1968).

[17] B. V. K. Vijaya Kumar and L. Hassebrook, "Performance measures for correlation filters," Appl. Opt. **29**, 2997–3006 (1990).

[18] J. L. Horner, "Light utilization in optical correlators," Appl. Opt. **21**, 4511–4514 (1982).

[19] Z. Zalevsky, D. Mendlovic, and H. J. Caulfield, "Fractional correlator with real-time control of the space-invariance property," Appl. Opt. **36**, 2370–2375 (1997).

[20] D. Mendlovic, Z. Zalevsky, A. W. Lohmann, and R. G. Dorsch, "Signal spatial-filtering using the localized fractional Fourier-transform," Opt. Commun. **126**, 14–18 (1996).

[21] Z. Zalevsky, D. Mendlovic, and H. J. Caulfield, "Localized partially space-invariant filtering," Appl. Opt. **36**, 1086–1092 (1997).

[22] A. Sahin, H. M. Osaktas, and D. Mendlovic, "Optical implementation of the two-dimensional fractional Fourier-transform with different orders in two dimensions," J. Opt. Soc. Am. A **12**, 134–138 (1995).

[23] D. Mendlovic, Y. Bitran, R. G. Dorsch, C. Ferreira, J. Garćia, and H. M. Ozaktas, "Anamorphic fractional Fourier transforming: optical implementation and applications," Appl. Opt. **34**, 7451–7456 (1995).

[24] J. García, D. Mendlovic, Z. Zalevsky, and A. Lohmann, "Space-variant simultaneous detection of several objects using multiple anamorphic fractional Fourier-transform filters," Appl. Opt. **35**, 3945–3952 (1996).

[25] A. W. Lohmann and D. Mendlovic, "Fractional joint transform correlator," Appl. Opt. accepted for publication.

[26] B. Javidi, "Nonlinear joint power spectrum based optical correlation," Appl. Opt. **28**, 2358–2367 (1989).

[27] A. Papoulis, *Probability, Random Variables, and Stochastic Processes* (McGraw-Hill, New York, 1984), pp. 215–283.

[28] J. L. Horner, "Clarification of Horner efficiency," Appl. Opt. **31**, 4629 (1992).

[29] J. L. Horner and P. D. Gianino, "Phase only matched filtering," Appl. Opt. **23**, 812–816 (1984).

[30] A. W. Lohmann, D. Mendlovic, and Z. Zalevsky, "Synthesis of pattern recognition filters for fractional Fourier processing," Opt. Commun. **128**, 199–204 (1996).

[31] D. Mendlovic, R. G. Dorsch, A. W. Lohmann, Z. Zalevsky, and C. Ferreira, "Optical illustration of a varied fractional Fourier-transform order and the Radon-Wigner display," Appl. Opt. **35**, 3925–3929 (1996).

[32] H. M. Ozaktas and D. Mendlovic, "Multistage optical implementation architecture with least possible growth of system size," Opt. Lett. **18**, 296–298 (1993).

[33] Y. Bitran, Z. Zalevsky, D. Mendlovic, and R. G. Dorsch, "Performance analysis of the fractional correlation operation," Appl. Opt. **35**, 297–303 (1996).

[34] A. Sahin, H. Ozaktas, and D. Mendlovic, "Optical implementation of the two-dimensional fractional Fourier-transform with different orders in the two dimensions," Opt. Commun. **120**, 134–138 (1995).

[35] J. Garcia, R. Dorsch, A. W. Lohmann, C. Ferreira, and Z. Zalevsky, "Flexible optical implementation of fractional Fourier transform processors. Applications to correlation and filtering," Opt. Commun. **133**, 393–400 (1997).

[36] D. Mendlovic, N. Konforti, and E. Marom, "Shift and projection invariant pattern recognition using logarithmic harmonics," Appl. Opt. **29**, 4784 (1990).

[37] A. W. Lohmann and D. P. Paris, "Binary Fraunhofer holograms, generated by computer," Appl. Opt. **6**, 1739–1748 (1967).

[38] F. T. S. Yu, S. Jutamulia, T. W. Lin, and D. A Gregory, "Adaptive real-time pattern recognition using a liquid crystal TV based joint transform correlator," Appl. Opt. **26**, 1370–1372 (1987).

[39] F. T. S. Yu and X. J. Lu, "A real-time programmable joint transform correlator," Opt. Commun. **52**, 10–16 (1984).

[40] A. W. Lohmann and B. H. Soffer, "Relationships between two transforms: Radon–Wigner and fractional Fourier," J. Opt. Soc. Am. A **11**, 1798–1801 (1994).

Optical pattern recognition

Edited by
FRANCIS T. S. YU
and
SUGANDA JUTAMULIA

CAMBRIDGE
UNIVERSITY PRESS

PUBLISHED BY THE PRESS SYNDICATE OF THE UNIVERSITY OF CAMBRIDGE
The Pitt Building, Trumpington Street, Cambridge, United Kingdom

CAMBRIDGE UNIVERSITY PRESS
The Edinburgh Building, Cambridge CB2 2RU, UK http://www.cup.cam.ac.uk
40 West 20th Street, New York, NY 10011-4211, USA http://www.cup.org
10 Stamford Road, Oakleigh, Melbourne 3166, Australia

First published 1998

Printed in the United States of America

Typeset in Times Roman 10/12.5 pt. in LaTeX 2_ε [TB]

A catalog record for this book is available from the British Library

Library of Congress Cataloging-in-Publication Data

Optical pattern recognition / edited by Francis T. S. Yu, Suganda Jutamulia.
p. cm.
ISBN 0-521-46517-6
1. Optical pattern recognition. I. Yu, Francis T. S., 1932– .
II. Jutamulia, Suganda.
TA1650.0655 1998 97-36651
621.39'9 – dc21 CIP

ISBN 0 521 46517 6 hardback

Contents